4

RESULTS AND DISCUSSION

Since the time immemorial medicinal plants have been used by mankind as a treatment to cure several diseases due to their therapeutic potential. They are able to produce a large number of diverse bioactive compounds, particularly secondary metabolites like flavonoids, alkaloids, terpenoids, tannins, and phenolic compounds (Asraoui *et al.,* 2021). Researchers are particularly interested in exploring the secondary metabolites of medicinal plants that are used in medicine for the treatment of diseases. The long process of isolating the suitable phytocompound with drug likeness and studying its biological property is reduced because of developments in the field of nanotechnology.

The usage of NPs in the management of many ailments is one of the aspects of nanomedicine, which is considered as the application of nanotechnology in medicine. Nanoparticles coated or coupled with various functionalities can be used to target the tumour site, which allows early diagnosis and elimination. Several noble metal NPs have been investigated for their anticancer potential, cellular imaging, and other oncological implications. Because of their enormous medical significance and potential to combat cancer, silver and its complexes have generated a lot of attention among noble metals. Although many chemical and physical methods are used to produce AgNPs, biological methods are less hazardous, environmentally friendly, and cost-effective. Plant extracts are preferred over other biosynthetic methods because they are readily available and include a diverse group of metabolites that favour the reduction of silver ions and speed up the synthesis process. Furthermore, the chemi-synthetic approach leaves harmful chemicals on surfaces, which might be hazardous in medical settings (George *et al.,* 2018).

Thus the present study involves the analysis and investigation of medicinal properties of plants and the efficacy of green synthesised silver nanoparticles using plants during diseased conditions. Enormous numbers of plant species have been studied for their pharmacological potential but still an infinite threatened species are unexplored. *Tabebuia* species have a long history of use as traditional medicine for treating cancer due to its phytoconstituent Lapachol and its derivatives from bark of the

tree (Subbiah and Krishnaswamy, 2017). However, there is a lack of comprehensive studies with regard to phytochemical characterization of *T. roseo-alba* and its therapeutic potential. Thus an attempt was made to elucidate the therapeutic potential of *T. roseo-alba,* synthesize silver nanoparticles using *T. roseo-alba and* investigate its antioxidant and anticancer potential in lung cancer cell lines *in vitro.*

The study was conducted in four phases and the results are furnished and discussed under the following headings.

Phase I

4.1 Phytochemical characterization and Assessment of Free radical scavenging potential of ethanolic extract of *T. roseo-alba* leaves

- 4.1.1. Preliminary phytochemical screening
- 4.1.2. Quantitative analysis of phytochemicals
- 4.1.3. High performance liquid chromatography
- 4.1.4. Gas chromatography–Mass Spectrometry Analysis
- 4.1.5. Assessment of Free radical scavenging potential of various extracts of *T. roseo-alba* leaves
  - 4.1.5.1. DPPH radical scavenging assay
  - 4.1.5.2. $ABTS^{+}$ radical scavenging Assay
  - 4.1.5.3. Hydroxyl radical scavenging assay
  - 4.1.5.4. Hydrogen peroxide radical scavenging Assay
  - 4.1.5.5. Nitric oxide scavenging assay
  - 4.1.5.6. Superoxide radical scavenging assay
  - 4.1.5.7. Reducing power assay

Phase II

4.2. Synthesis and Characterization of the AgNPs of *T. roseo-alba*

- 4.2.1. Synthesis of AgNPs of *T. roseo-alba*
- 4.2.2. Characterization of AgNPs of *T. roseo-alba*
  - 4.2.2.1. UV-Visible Spectroscopy
  - 4.2.2.2. Fourier Transform Infrared spectroscopy
  - 4.2.2.3. Dynamic light Scattering
  - 4.2.2.4. Zeta-Potential
  - 4.2.2.5. X-RAY Diffraction analysis
  - 4.2.2.6. Energy Dispersive Spectroscopy

4.2.2.7. Scanning electron microscope

4.2.2.8. Transmission Electron Microscope and Selected Area Electron Diffraction

Phase III

4.3 Evaluation of Anticancer potential and *in vitro* cytotoxicity of ethanolic extract of *T. roseo-alba* and its biosynthesized AgNPs

4.3.1 MTT Assay

4.3.2 Determination of Apoptosis by Flow cytometer-Kit method

4.3.2.1. Analysis of Apoptosis by Annexin V/FITC staining

4.3.2.2. Analysis of Mitochondrial Membrane Potential by JC-1 staining

4.3.2.3 Analysis of DNA Fragmentation

4.3.2.4 Western Blot Analysis

4.3.3. Cell cycle Analysis-Kit method

Phase IV

4.4. *In Silico* analysis

4.4.1. ADMET Analysis

4.4.2. Molecular docking

Phase I

4.1 Phytochemical characterization and Assessment of Free radical scavenging potential of ethanolic extract of *T. roseo-alba* leaves

Extraction yield

The leaves of *T. roseo-alba* were extracted with various solvents of different polarities like chloroform, petroleum ether, ethanol and water. The solvents were selected based on their polarity and solubility of the active compounds present in the sample. Percentage yield of the various extracts was calculated and presented in Table 1.

Table 1. Extraction yield of *T. roseo-alba* leaves

Solvents	Petroleum Ether	Chloroform	Ethanol	Water
Yield (%)	3.58	7.15	**11.52**	8.05

It is evident from the results that the highest yield was obtained in ethanolic extract when compared with other solvent extracts of *T. roseo-alba* leaves. The percentage of yield in other extracts namely petroleum ether, chloroform and water was

found to be 3.58, 7.15, 8.05 percent respectively indicating the presence of more hydrophilic phytoconstituents in the plant sample. Several parameters, such as the quality of phytochemicals, the process used for extraction, the particle size, the solvent used and the effect of nosy substances, influence the efficiency of extraction (Do *et al.,* 2014). Owolabi *et al.* (2018) also analysed the effect of various solvents on the extraction yield and reported the presence of various phytochemical constituents in all the solvent extracts of *Feretia apodanthera root bark extracts.* The yield of plant extract in *Carica papaya* leaves using different solvents was assessed by Sheneni *et al.* (2018) and the higher percentage of yield was obtained in ethanolic extract and methanolic extract of *Carica papaya* leaves. The percentage yield of *Leea indica* leaves using different solvents was analysed by Ghagane *et al.* (2017) and the percentage yield obtained in ethanolic extract of *Leea indica* leaf was found to be 16.52g. The findings of the current study are in par with the report observed by Leela and Singh, (2020) where the maximum yield was obtained using ethanolic extract with all the three medicinal plants *Lawsonia inermis*, *Mangifera indica* and *Piper betel* leaves analysed.

4.1.1. Preliminary phytochemical screening

Medicinal plants are considered as an integral part of human evolution because, even in this modern period, more than 75% of the World's population relies on medicinal plants for a variety of health issues. The medicinal properties of plants can be ascribed to the bioactive components such as carotenoids, phenolic acids, flavonoids and they have been found to exhibit efficient antioxidant properties along with other biological abilities (Nazir *et al.,* 2021)**.**

The present study on the phytochemical analysis revealed the existence of various bioactive metabolites like phenols, flavonoids, saponins, alkaloids and terpenoids (Table 2). From the results, it was apparent that though all the extracts were found to contain active metabolites, ethanolic extract was found to have most of the bioactive compounds. Diverse group of phytochemicals have been identified in the family of Bignociacea. Various phytochemicals like reducing sugars, organic acids, alkaloids, depsides and depsidones, foamy saponins, phenols and tannins have been identified from the study on *Tabebuia serratifolia* by Silva *et al.* (2017). Similar work has also been carried out by Souza *et al.* (2020) on phytochemical analysis and evaluation of *Chaptalia nutans* (L.) for *in vitro* antioxidant and cytotoxic potential, who reported the presence of various metabolites like total phenols, alkaloids, total flavonoids, saponins,

tannins and ascorbic acid. The phytochemical analysis of *Ephedra intermedia* extract evidenced the existence of various bioactive components such as reducing sugars, phenolic compounds, cardiac glycosides, flavonoids, and alkaloids (Gul *et al.,* 2017)**.** The phytochemical analysis of *O. sanctum* leaf extract, documented the existence of several phytochemicals like phenols, flavonoids and tannin compounds (Panchal and Parvez, 2019). In a study by Dharmapal *et al.* (2018), the results revealed the presence of diverse phytochemicals in stem extracts of *Fibraurea darshani*.

Thus it can be inferred from the results of phytochemical analysis that the ethanolic extract of *T. roseo-alba* can be a good source of secondary metabolites including alkaloids, flavonoids, phenols, saponins, terpenoids which might contribute for the therapeutic efficacy of the candidate plant.

Table 2. Phytochemical screening of ethanolic extract of *T. roseo-alba* leaves

Compound	Petroleum ether	Chloroform	Ethanol	Aqueous
Alkaloids	-	-	+	+
Flavonoids	+	+	+	-
Saponins	-	-	+	+
Carbohydrates	-	+	-	-
Proteins	-	-	+	-
Phenols	+	+	+	+
Glycosides	-	-	+	-
Tannins	-	-	+	+
Terpenoids	-	+	+	-

Note: "+"- Presence of Phyto constituents; "-"- Absence of Phyto constituents

4.1.2. Quantitative analysis of phytochemicals

Medicinal plants play an important role in human life for promoting good health due to the presence of bioactive phytochemicals. They have long been used to treat infections, and a number of natural compounds are employed as phototherapeutics to treat a variety of ailments (Bhargava *et al.,* 2021). The amount of proteins, carbohydrates, phenols, flavonoids and tannins are tabulated in Table 3. When compared to other

phytoconstituents, Total phenolic content was found to be greater (112.67±0.03 mg GAE/g) in the ethanolic extract of *T. roseo-alba* leaves. The antioxidant activity of the selected medicinal plant could be ascribed to the presence of phenol and flavonoids.

Table 3. Quantitative Phytochemical analysis of ethanolic extract of *T. roseo-alba* leaves

Bioactive compounds	Ethanolic extract
Total Protein (mg/g)	26.23 ± 0.08
Carbohydrates (mg/g)	22.36 ± 0.12
Total Phenols (mgGAE/g)	112.67 ± 0.03
Total Flavonoids (mg quercetin equivalents/g)	12.54 ± 0.24
Tannins (mg/g)	10.34 ± 0.67

The results are in concordance with Bains *et al.* (2020) who quantified active metabolites in various extracts of *Madhuca longifolia* and *Punica granatum* and highest phenolic content was reported in methanolic extract. Various phyto constituents like saponins, flavonoids, phenols and alkaloids were quantified in the ethanolic extract of *Citrus paradise* by Roghini and Vijayalakshmi, 2017. Yadang *et al.* (2019) observed higher levels of total phenolic content in water and methanolic extracts of *Carissa edulis* Valh. (Apocynaceae) leaves. The bioactive phytoconstituents such as phenols, flavonoids, alkaloids and tannins have been proved to be the scavengers of free radicals, lipid peroxidation inhibitors, and these compounds have important properties such as anticancer, anti-oxidant, antiglycemic, wound healing, analgesic, and anti-inflammatory (Divya and Kalaiselvi, 2017).

The qualitative and quantitative phytochemical analysis of the present study clearly evidenced the presence of several phytoconstituents in the leaves of *T. roseo-alba*. Further, it becomes imperative to analyse the major phytoconstituents of the plant sample. Hence, advanced chromatographic separation methods were adopted as given below.

4.1.3. High performance thin layer chromatography

Plant derived bioactive compounds with a variety of pharmacological activities are lead molecules for the development of therapeutic drugs. Their scientific validation is therefore important for ensuring reliability and therapeutic effectiveness. The first step towards understanding the types of active principles present in a plant is the study of HPTLC. The chemical fingerprints produced by chromatographic methods are an approach to identify the various phytoconstituents dispersed in the plant material and to maintain the "database" for future studies (Kuruvilla *et al.,* 2019). HPTLC profiles are developed in the pharmaceutical industries as a valuable quality assessment tool due to reliability, precision, cost effectiveness, and function as a phytomarker /metabolites marker or chemical fingerprint to classify, authenticate herbal drugs (Johnson *et al.,* 2020). HPTLC profile was generated for ethanolic extract of *T. roseo-alba* leaves in different solvent systems of differing polarity in order to determine the presence of active metabolites.

HPTLC chromatogram displayed for phenolic profile of the ethanolic extract of *T. roseo-alba* was shown in Plate 2 and Figure 16. The profile was generated along with the standard compound Quercetin. The chromatogram was run using the mobile phase comprising Toluene:acetone: formic acid in the ratio and developed by spraying with folin ciocalteu reagent followed by 1% ethanolic aluminum chloride. In the chromatogram blue color bands observed under UV light after derivatization revealed the occurrence of polyphenols and it was compared with the standard. The HPTLC profile reveals the presence of several phytoconstituents as indicated by the presence of many bands in the plant sample tested. From the Rf value obtained for the Quercetin standard, it can be interpreted that the candidate plant may be a source of quercetin-like compounds as the lane loaded with *T.roseo-alba* sample had intense band formation with the same Rf value.

A similar work has been carried out by Savadi *et al.* (2020) and 17 chemicals with hydroxyl groups were identified in the methanolic extract of *C. dactylon* rhizomes. Phenolic compounds are a type of secondary metabolite that protects tissues from oxidative stress caused by reactive free radicals, and thus they help to prevent diseases including inflammatory disorders, cancer, diabetes, myocardial infarction, Alzheimer's disease, and Parkinson's disease. The antioxidant potential of the plant extract is generally assessed by the presence of phenols, flavonoids, isoflavonoids, and anthocyanins.

Numerous studies have revealed a direct link between the antioxidant potential of plant extracts and the concentration of phenolic chemicals and flavonoids in plants (Zagórska-Dziok *et al.,* 2020).

Plate 2. HPTLC finger printing profile for phenols

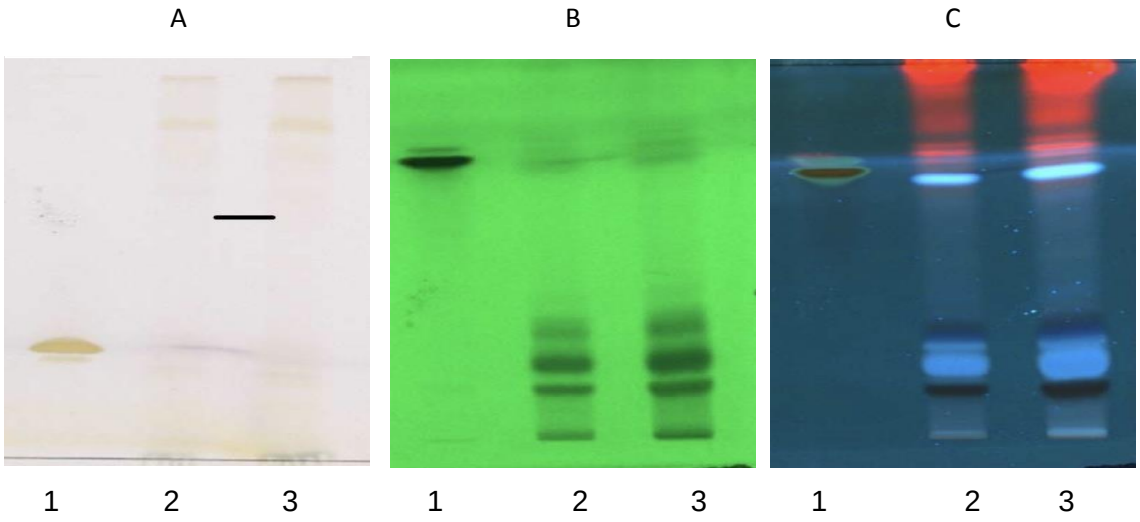

Lane 1 = Standard Quercetin Lane 2 and 3 = *T. roseo- alba* sample

A Before derivatization: under day light, **B** Before derivatization:under UV 254 nm, **C** After derivatization: under 366 nm**.**

Figure 16. Baseline display and Peak densitogram display for phenol

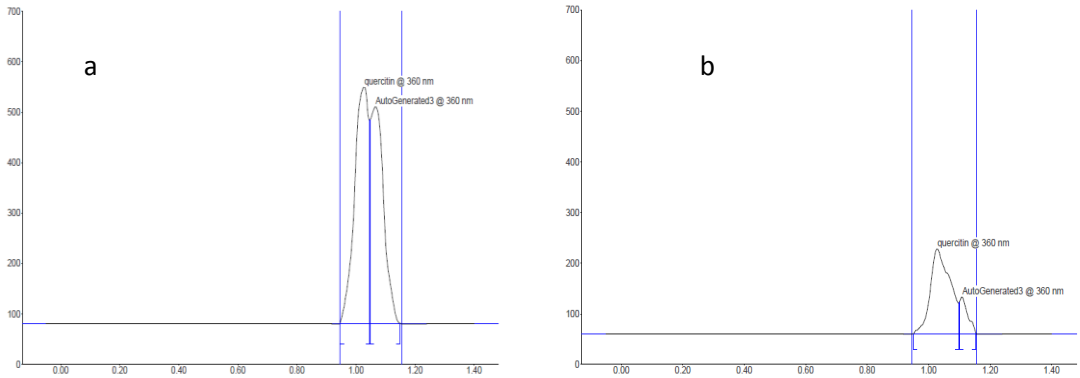

a. Standard (Quercetin) b. ethanolic extract of *T. roseo-alba*

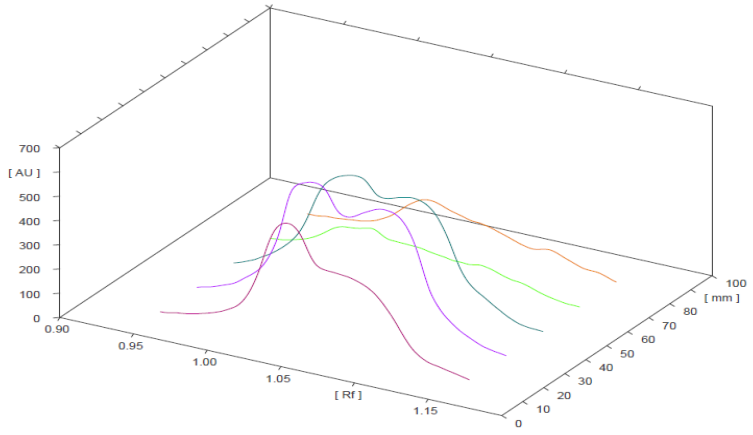

3 D display of all tracks

For generating HPTLC flavonoid profile, the chromatogram was run using the mobile phase comprising toluene:ethyl acetate:formic acid in the ratio 5:4:0.2 and developed by spraying with 5% methanolic sulphuric acid. HPTLC flavonoid profile of the ethanolic extract of *T. roseo-alba* exhibited 14 peaks, among them max Rf value 0.32 and max Rf value 1.05 matched with max Rf of standard Rutin and Kaempferol respectively which confirmed the presence of flavonoids like Rutin and Kaempferol**.** Densitogram and 3D display for a flavonoid profile was documented in Plate 3 and Figure 1**7**. Yellow and yellowish blue coloured fluorescent zone at the UV 366 nm mode after derivatization validated the existence of flavonoids in the plant sample.

Plate 3. HPTLC fingerprinting profile for Flavonoids

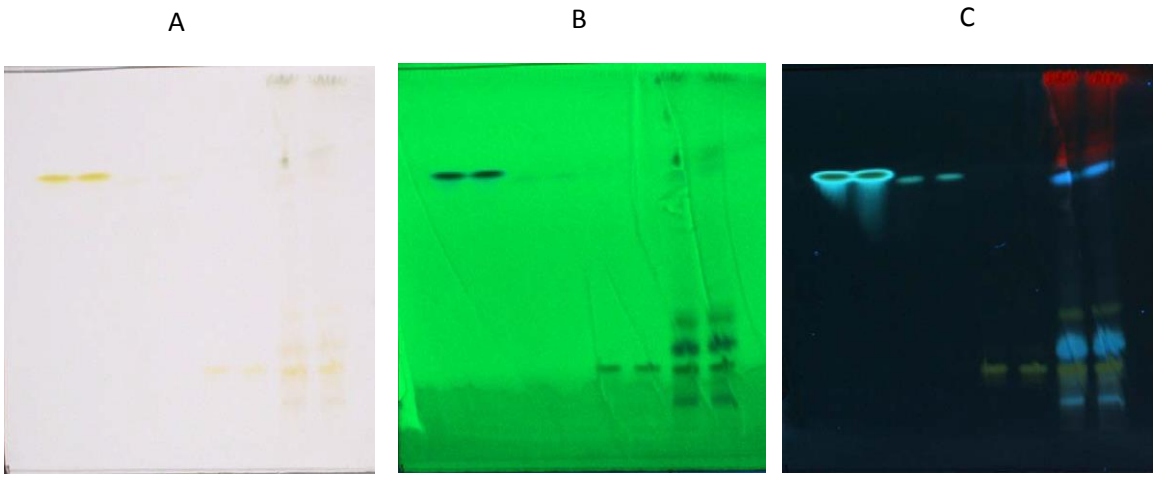

Lane 1 and 2 = Kaempferol, Lane 3 and 4= Quercetin, Lane 5 and 6= Rutin Lane 7 and 8 = Plant sample

A Before derivatization: under daylight, **B** Before derivatization:under UV 254 nm, **C** After derivatization: under 366nm.

Figure 17. Baseline display and Peak densitogram display for Flavonoid

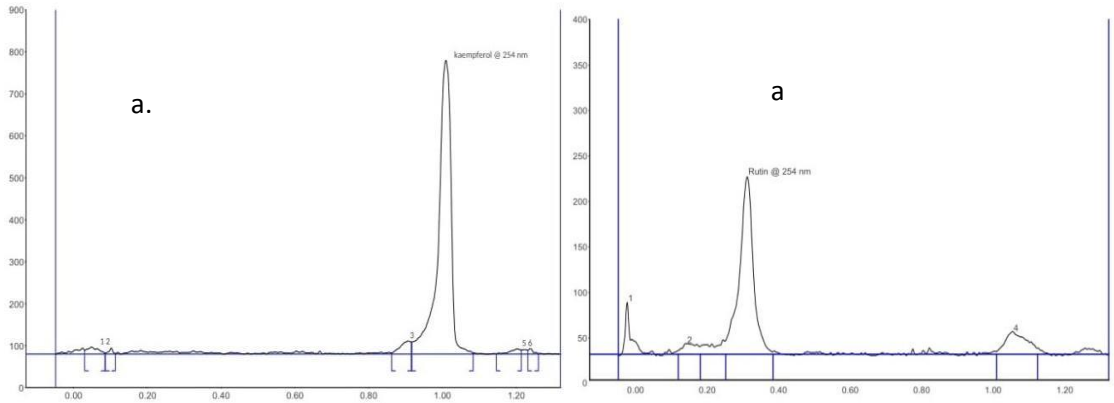

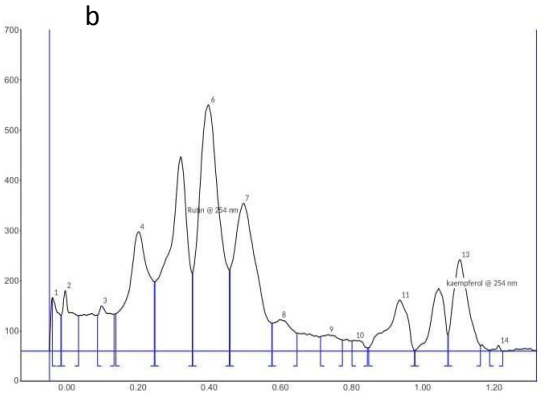

a. Standards (Kaempferol and Rutin) b. ethanolic extract of *T. roseo-alba,*

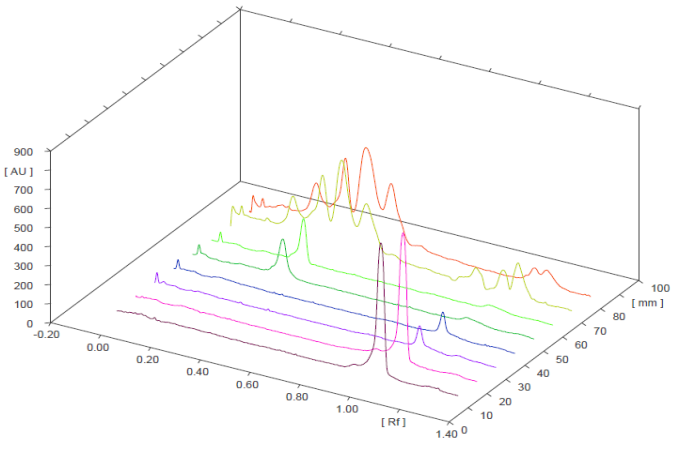

3D display of all tracks

Similar to our study, the presence of flavonoids were recorded by Jaafar *et al.* (2020) in the ethyl acetate and n-butanol fractions of *Euphorbia cyathophora*. Hemmalakshmi *et al.* (2016) identified flavonoids in ethanolic extract of *Erythrina variegate* L. flowers by HPTLC fingerprinting analysis. HPTLC profiling was produced using *Morus alba Linn.* (White mulberry) ethanolic leaf extract and various peaks, bands corresponding to flavonoids and phenolics have been detected and quantified (Ali *et al.,* 2020). High performance thin layer chromatography analysis carried out by Pallavi and Hemalatha, (2018) documented the existence of rutin and quercetin in the ethanolic leaf extract of *Calamus rotang* Linn**.**

Besides therapeutic substances, medicinal plants are a rich source of information on a wide range of phytoconstituents that might be used as medications with precision. These are the sources of potentially important therapeutic compounds that could provide novel clues and insights for drug discovery in the modern era. The most significant of these phyto constituents include phenolic compounds, flavonoids, alkaloids and tannins (Sujatha *et al.,* 2017). Flavonoids are considered as the most important natural phenolic compounds since they have been explored as anticancer, antibacterial, antiviral, antiangiogenic, antimalarial, antioxidant, neuroprotective, antitumor, and anti-proliferative agents (Ullah *et al.,* 2020).

HPTLC profile of the ethanolic extract of leaves of the study plant for alkaloids was recorded in Plate 4 and Figure 18. The chromatogram was run along with the mobile phase containing ethyl acetate-methanol-water in the ratio 10:1.35:1 and after derivatization with Dragendorff reagent followed by 10% ethanolic sulphuric acid it was photo documented. Alkaloid profile of the plant sample evidenced the presence of 3 peaks among which Peak 1 with max Rf 0.90 unveiled the presence of Colchicine. Yellow brown coloured zones at day light mode were observed in standard and plant sample tracks and this validated the presence of alkaloids in the leaves of *T. roseo-alba.*

Plate 4. HPTLC fingerprinting profile for Alkaloids

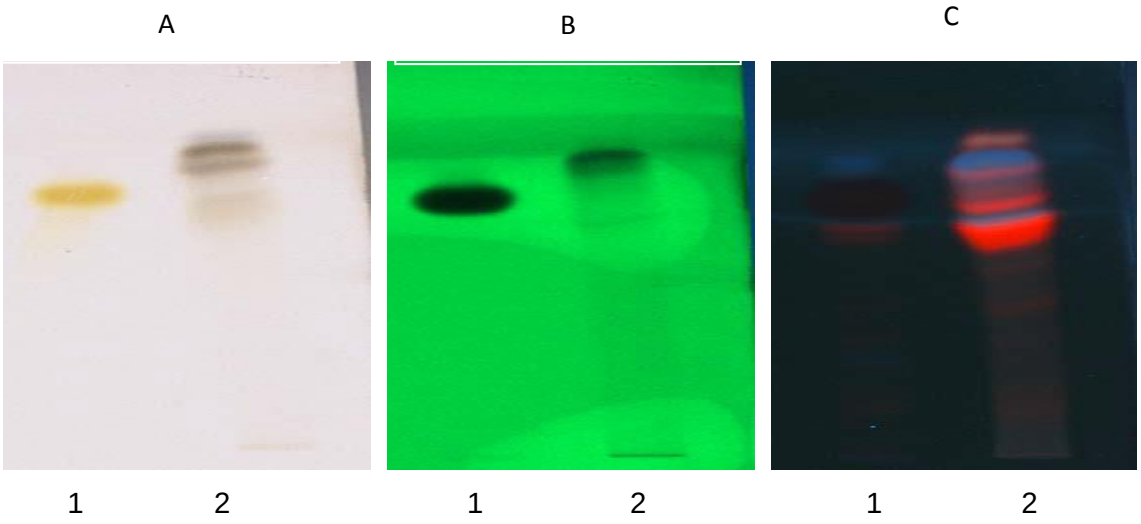

Lane 1 = Colchicine Lane 2= Plant sample

A Before derivatization: under day light, **B** Before derivatization:under UV 254 nm, **C** After derivatization**:** under 366nm.

Figure 18. Baseline display and Peak densitogram display for Alkaloids

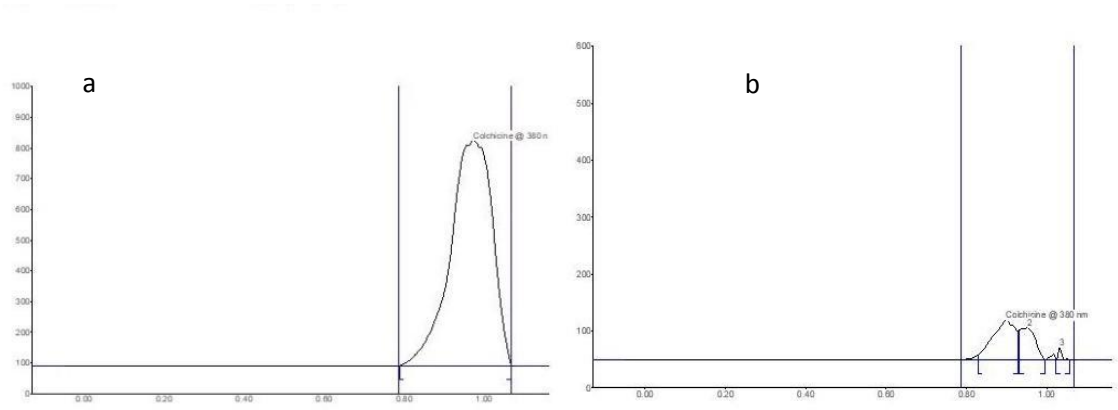

a. Standard (Colchicine) and b. ethanolic extract of *T. roseo-alba*

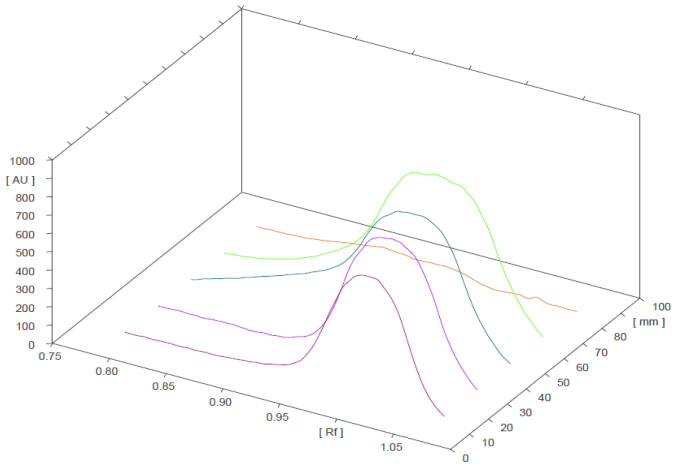

3 D display of all tracks

Taheri *et al.* (2021) showed the existence of flavonoids, terpenoids, alkaloid compounds, in the ethanolic extract of *Pyracantha coccinea* M. Roem. using HPTLC profile. In another study, Varkey and Kasthuri, (2016) demonstrated similar results with *Terminalia chebula,* the presence of alkaloids were documented based on the colour bands observed. HPTLC fingerprinting of petroleum ether extract of *Holoptelea integrifolia* (Roxb.) Planch leaves were performed to reveal the existence of alkaloids using the toluene-ethyl acetate-dimethylamine solvent system. HPTLC chromatogram when observed at wavelength 366 nm showed the presence of various bands corresponding to alkaloids (Sutar *et al.,* 2016). Kale and Patil, (2021) analysed the active principles present in methanolic extract of *Piper betle* leaves and HPTLC profile illustrated the presence of diverse phytochemicals including, phenols, flavonoids and alkaloids. The HPTLC analysis of different extracts from *C. latifolia* stem with different solvent systems showed several peaks and the HPTLC profile showed the presence of a range of active components (Kuruvilla *et al.,* 2019).

Alkaloids are the nitrogenous compounds originating in the plant kingdom which include amino acids and other nitro compounds. They are primarily considered as the rich source of medicinal uses such as analgesic, and adaptogenic activities that help to lighten pain, improve disease tolerance, stress resistance, and cure many diseases (Senguttuvan and Subramaniam, 2016). Furthermore, studies have demonstrated that alkaloids in plants can have a hypoglycemic effect through an insulin-releasing mechanism and insulin-mimicking activity, reducing postprandial hyperglycemia (Sagbo *et al.,* 2020)**.**

Tannin chromatogram was run along with the mobile phase containing Toluene-ethyl acetate-formic acid-methanol in the ratio 3:3:0.8:0.2 and after derivatization with 5% alcoholic ferric chloride, it was photo documented. HPTLC data of ethanolic leaf extract for tannins at 254 nm showed the presence of 12 peaks (Plate 5 and Figure 19) out of which one Max Rf value, 0.78 was matched with the Max Rf value of standard Gallic acid. Apparently, the desired profile was attained in the mobile phase toluene-ethyl acetate-formic acid-methanol (3:3:0.8:0.2).

Plate 5. HPTLC fingerprinting profile for Tannins

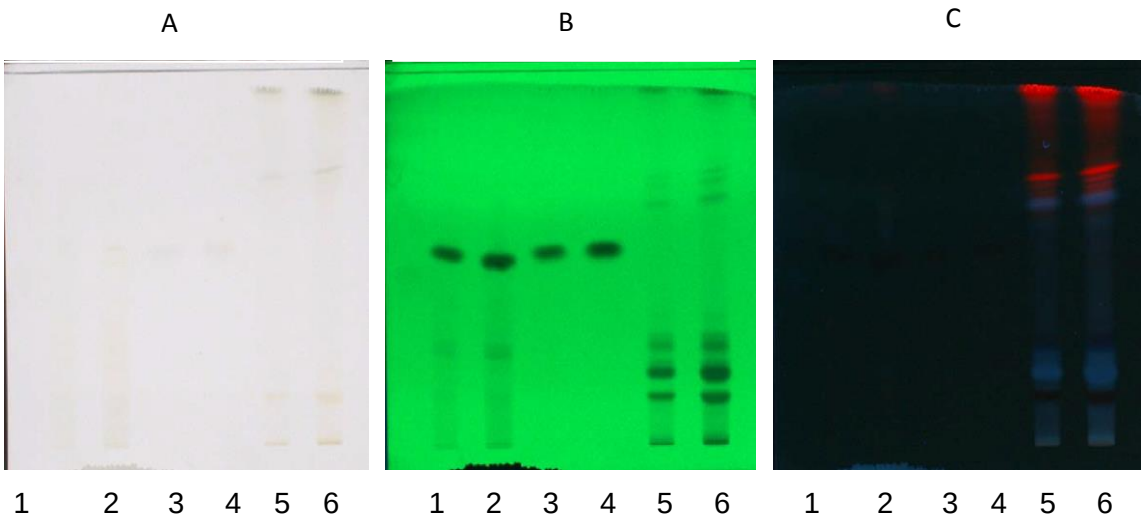

Lane 1 and 2 = Catechine, Lane 3 and 4= Gallic acid Lane 5 and 6= Plant sample

A Before derivatization: under day light, **B** Before derivatization:under UV 254 nm, **C** After derivatization: under 366nm.

Figure 19. Baseline display and Peak densitogram display for Tannins

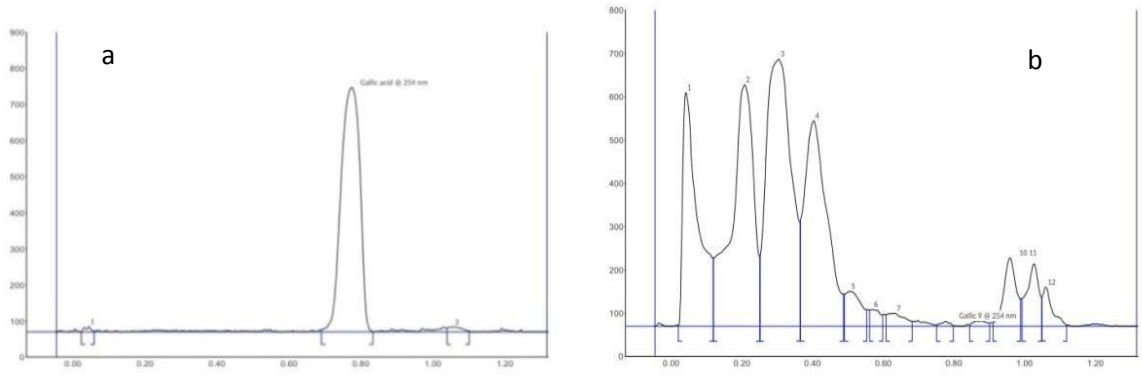

a. Standard (Gallic acid) and b. ethanolic extract of *T. roseo-alba*

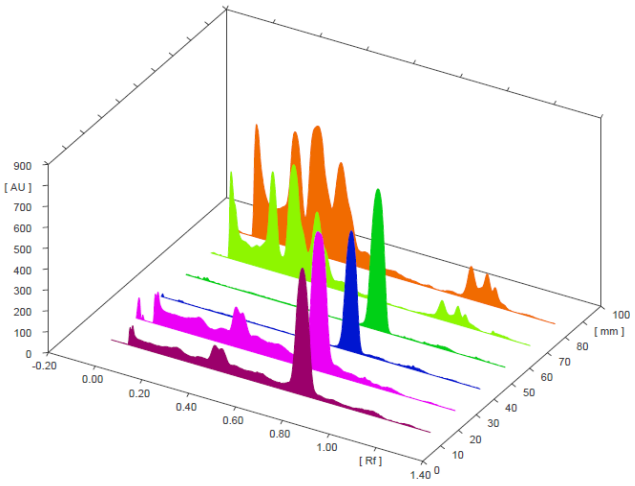

3 D display of all tracks

The results from HPTLC fingerprint of *A. aethiopicum* leaves using toluene-ethyl acetate-formic acid-methanol (3:3:0.8:0.2) evidenced the presence of gallic acid and tannin (Johnson *et al.,* 2020). A study carried out by Jyothisree and Umadevi, (2020) with newly formulated arishta from *Ficus religiosa* root bark demonstrated the occurrence of different types of tannins at different Rf values indicating the presence of gallic acid derivatives. Similar to our results, Narayanan and Antonysamy, (2016) reported the presence of tannins in selected *Cyathea* species from Western Ghats using HPTLC fingerprinting profile. The existence of various types of tannins with Rf values ranging from 0.07 to 0.93 were evidenced from HPTLC chromatograms of *A. lanata* ethanol extract by Sounder and Doss, (2017).

Tannins are polyphenolic chemicals found in plants which have powerful antibacterial, antiviral, antifungal, antiparasitic properties and also have anti-cancer and cytotoxic properties (Batool *et al.,* 2019). The therapeutic potential of medicinal plants in the treatment of some diseases is due to the presence of tannins. They are also reported to have diverse physiological effects like antimicrobial, anti-inflammatory, antidiabetic and antioxidant effects (Maisetta *et al.,* 2019).

To conclude, various bioactive phyto constituents like phenols, flavonoids, alkaloids and tannins have been identified from HPTLC fingerprinting analysis. It can be inferred from the results that the biopotency of *T. roseo-alba* may be due to the cumulative effects of these active metabolites.

4.1.4. Gas chromatography–Mass Spectrometry Analysis

GC-MS is one of the most widely used methods for determining phytochemical composition. By comparing the relative retention times, indices and their mass spectra, the identification of the specific natural compounds found in a plant extract is possible (Padma *et al.,* 2020). It is one of the best ways to ascertain the components like branched chain hydrocarbons, volatile matter, esters, and alcoholic acids (Iftikhar *et al.* 2019) merges two diagnostic methods to a distinct technique for analyzing mixtures of compounds. The components of the mixture are separated by Gas chromatography and each of the components can be analysed separately by mass spectroscopy (Sunitha *et al.,* 2017).

GC-MS chromatogram of the ethanolic extract of *T. roseo-alba* is depicted in Figure 20. By comparing the mass spectra of the constituents with the NIST 8 and WILEY 8 library, eight peaks were obtained in GC at retention times 22.36, 23.24, 27.68, 38.51, 39.08, 44.51, 44.80 and 51.56 minutes. From these, various phyto constituents were identified based on the comparison of the mass spectra constituents with the NIST library (Table 4 and 5). The main compounds that were identified from the GC-MS spectra include Squalene and Spinacene at retention time 39.08, isomers of Phytol at retention time 27.68, Stigmasterol, Alpha-dihydro fucosterol and sitosterol at retention time 51.56. Phytol and its isomers were found to be identified twice at two different retention times. The highest peak area (%) of 16.21 and 12.42 was obtained by Stigmast-5-en-3-ol, (3, Beta) at the retention time of 51.13 and 51.567 minutes respectively.

Figure 20. GC-MS Analysis of ethanolic extract of *T. roseo-alba* leaves

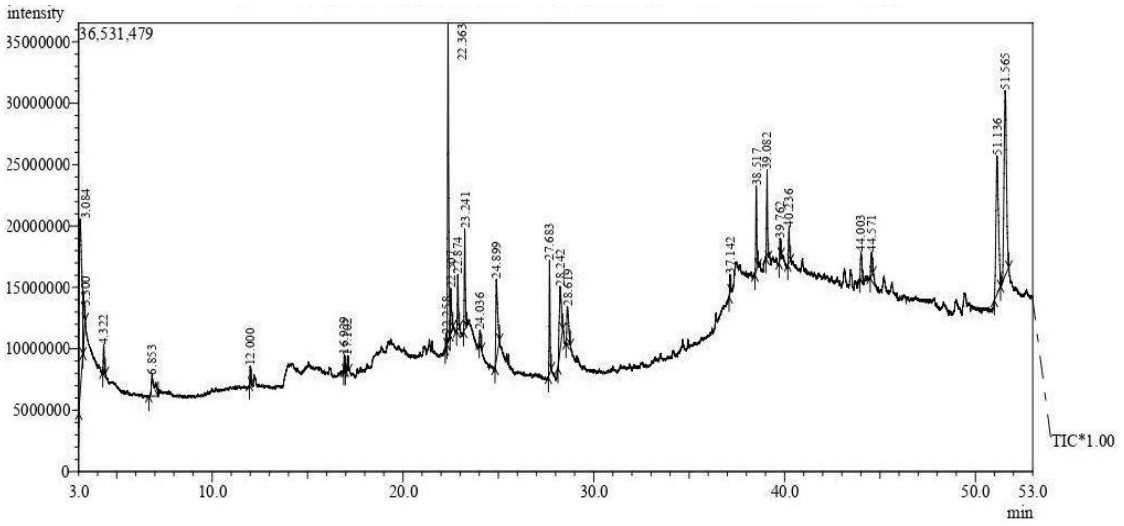

Table 4. Bioactive constituents identified in ethanolic extract of *T. roseo-alba* leaves by GC-MS analysis.

S.No	RT	Molecular formula	Molecular Weight	Name of the Compound
1.	22.367	$C_{20}H_{40}O$	296	2-Hexadecen-1-ol, 3,7,11,15,-Tetramethylhexadec-2-en-1-ol 3,7,11,15-tetramethyl-2-hexadecen-1-ol
2.	22.508	$C_{20}H_{40}$	280	2-Hexadecene 3,7,11,15-tetramethyl-[R-[R*R*-(E)] 3,7,11,15-Tetramethyl-2-hexadecene
3.	24.900	$C_{18}H_{34}O_2$	282	9-Octadecenoic acid (Z) Octadec-9-enoic acid
4.	27.683	$C_{20}H_{40}O$	296	Phytol 2-Hexadecen-1-ol Trans – Phytol 3,7,11,15-Tetra methyl-2-hexadecen-1-ol
5.	28.242	$C_{20}H_{34}O_2$	306	8,11,14- Eicosatrienoic acid (Z,Z,Z)
6.	39.083	$C_{30}H_{50}$	410	Squalene 2,6,10,14,18,22-Tetracosahexaene Spinacene
7.	51.136	$C_{29}H_{50}O$	414	Stigmast-5-en-3-ol (3.BETA.,24S) Stigmast-5-en-3-ol Beta-Sitosterol Stigmast-5-en beta-ol Alpha-Dihydrofucosterol
8.	51.567	$C_{29}H_{50}O$	414	Stigmast-5-en-3-ol (3.BETA.,24S) Stigmast-5-en-3-ol

Table 5. Biological activities of the phytoconstituents identified in ethanolic extract of *T. roseo-alba* leaves by GC-MS analysis.

S.No	% Area	Name of the Compound	Biological Activity**
1.	12.57	2-Hexadecen-1-ol 3,7,11,15,-Tetramethylhexadec-2-en-1-ol 3,7,11,15-tetramethyl-2-hexadecen-1-ol	Antimicrobial, Anticancer, Anti-inflammatory, Diuretic
2.	2.01	2-Hexadecene 3,7,11,15-tetramethyl-[R-[R*R*-(E)] 3,7,11,15-Tetramethyl-2-hexadecene	Transplant rejection treatment, Anticarcinogenic, Multiple sclerosis treatment, Gaucher disease treatment, Metabolic disease treatment.
3.	5.18	9-Octadecenoic acid (Z) Octadec-9-enoic acid	Cancer preventive, Flavor, Hypocholesterolemic, 5-Alpha reductase inhibitor, Antiandrogenic, Perfumery, Insectifuge, Anti-inflammatory, Anemiagenic, Dermatitigenic, Choleretic.
4.	3.54	Phytol 2-Hexadecen-1-ol Trans – Phytol 3,7,11,15-Tetra methyl-2-hexadecen-1-ol	Pesticide, perfumery, Anti-feedent, Haepato protective, anti-inflammatory, Analgesic, Antibacterial activity.
5.	4.80	8,11,14- Eicosatrienoic acid (Z,Z,Z)	Cardio protective, Hypocholesterolemic, Anticancer, Anticoronary.
6.	2.85	Squalene 2,6,10,14,18,22-Tetracosahexaene Spinacene	Antibacterial, Antitumor, Antioxidant, immunostimulant, hypocholesterolemic, Lipoxygenase-inhibitor.
7.	12.42& 16.21	Stigmast-5-en-3-ol (3.BETA.,24S) Stigmast-5-en-3-ol Beta-Sitosterol Stigmast-5-en beta-ol Alpha-Dihydrofucosterol	Cytotoxicity against human, diuretic, hepatoprotective, anti-microbial, anti-inflammatory, anticancer, antiasthma.

Similar to this study, (Subramanian *et al.,* 2020) have identified 38 phyto compounds with natural antioxidant potential in *Gymnema sylvestre* using gas chromatography-mass spectrometry. The research work by Ramalakshmi and Muthuchelian, (2011) on GC–MS study of *Tabebuia rosea* (Bertol.) ethanolic extract showed the presence of 18 bioactive components in the plant. In tune with the present study, the investigation reports the GC-MS analysis of quinoa (*Chenopodium quinoa* Willd.) root extract revealed the presence of a diverse group of phyto compounds (Khan *et al.,* 2020). GC-MS analysis of *Pergularia daemia* leaves revealed the existence of seventeen phytochemical constituents (Rukshana *et al.,* 2017).

Natural compounds originally derived from plants are considered as useful pharmacological sources and contribute to the therapeutic potential of the plant (Jayakar *et al.,* 2020). Phytol, 3,7,11,15- Tetramethyl-2-hexadecen-1- ol, a monounsaturated acyclic diterpene known to possess anticancer, anti-inflammatory, antidiuretic, antimicrobial, antioxidant, immunostimulant and cholesterol lowering properties. Terpenes and terpenoids play essential physiological and ecological roles, and they have extensive biological actions, including hepatoprotective, antioxidant, and cholinesterase inhibitor activity (Bano and Deora, 2020).

Squalene, a triterpene, was proven to exhibit antioxidant, chemopreventive, antitumor and hypocholesterolemic activities. Phytosterols such as α-sitosterol and β-sitosterol inhibit carcinogenesis by directing different mechanisms that lead to cancer. By enhancing antioxidant enzymes and lowering reactive oxygen species generation and oxidative stress, they were able to prevent angiogenesis. These sterols, inhibited the production of inflammatory cytokines and induced apoptosis. In addition, stigmasterol is a precursor for semisynthetic progesterone, a valuable human hormone implicated in oestrogen-related regulation and tissue-repairing mechanisms, and frequently serves as an intermediary compound in the production of sex hormones and corticoids. It is also involved in the production of vitamin D3 (Casuga *et al.,* 2016).

Oleic acid or 9-Octadecenoic acid, a monounsaturated fatty acid, is found to have anti-inflammatory, cancer preventive, anti-androgenic, 5-alpha reductase inhibitor, anemiagenic, insectifuge, dermatitigenic and hypocholesterolemic properties (Choudhary *et al.,* 2019). β-sitosterol, the steroid compound, is found to contain different biological activities like antitumor, antiproliferative, antioxidative, antiviral, immunomodulatory and hepatoprotective activity (Parvez *et al.,* 2018).

Thus the findings of the current study justified the therapeutic potential of *T. roseo-alba* owing to the presence of various pharmacologically active compounds. Since chromatographic analysis was the primary attempt for studying the nature of active compounds in the plant, further research in the candidate plant is required for the development of novel drugs and to explore its pharmacological potential and thus an attempt was made to confirm its radical scavenging potential.

4.1.5. Assessment of Free radical scavenging potential of various extracts of *T. roseo-alba*

Free radicals are produced as the by-products of oxidative metabolism and also by exposure to environmental insults such as pathogenic agents, pollution, ultraviolet light, and radiation in all living organisms. They are highly unstable and can promptly react with most of the biological macromolecules, comprising proteins, lipids, lipoproteins and nucleic acids. Excess amount of ROS can produce oxidative stress and cause cellular or tissue damage, which is linked to most of the degenerative diseases like ageing, diabetes, cardiovascular disease, neurodegenerative illness, inflammation, atherosclerosis, carcinogenesis, and mutagenesis (Zhou *et al.,* 2020). The formation of these free radicals in a normal healthy human body is effectively regulated by several antioxidant protection mechanisms such as superoxide dismutase (SOD), catalase, glutathione peroxidases and reductase, vitamin E (tocopherols and tocotrienols) and vitamin C (Naidu *et al.,* 2017). Antioxidants are chemical substances that aid in the inhibition of oxidation reactions produced by free radicals and protect the cells by various mechanisms like converting ROS to non-radicals, and breaking of auto oxidative chain reaction (Lourenço *et al.,* 2019). They also serve as reducing agents, free radical scavengers and quenchers of singlet oxygen molecules, and antioxidant enzyme activators to regulate the harm caused by free radicals in living systems (Israel, 2017).

Various synthetic antioxidant chemicals such as butylated hydroxyanisole (BHA), butylated hydroxytoluene (BHT), and propyl gallate have been widely used to treat the consequences of oxidative stress. Despite their widespread use, they have been linked to adverse consequences such as hepatotoxicity and carcinogenicity. Therefore, recently studies have been focused on developing ethnomedicinal compounds with strong antioxidant activities but low cytotoxicity to substitute synthetic antioxidants (Guchu *et al.,* 2020). Many bioactive components found in plants serve as radical scavengers and can be used as medicines (Kaur and Saxena, 2020).

These phytochemical compounds, such as flavonoids and other phenolic components, have been shown to be potent antioxidants, anticancer, antibacterial, and cardioprotective agents, and may be useful as pharmaceutical and medicinal candidates (Tungmunnithum *et al.,* 2018). Natural antioxidants are potentially safe since they have few adverse effects, effective in terms of efficacy, and economical because they are derived from renewable resources (Nazir *et al.,* 2021).

Previous research has also indicated that certain plant extracts have high antioxidant activity, suggesting that they may be useful in preventing oxidative damage in the body (Mbaoji and Nweze, 2020). Since *Tabebuia* species has established to be the rich source of many organic compounds, in particular, phenolic and polyphenolic compounds (Govindappa *et al.,* 2013) the current study is formulated to assess the free radical scavenging activities of different extracts of *T. roseo-alba* leaves and all findings were compared with the standard.

4.1.5.1. DPPH radical scavenging assay

DPPH is a nitrogen-centered radical with a characteristic absorption at 517 nm, commonly used for assessing the radical scavenging activity of plant extracts and to assess the capacity of compounds as free-radical scavengers or hydrogen donors. When antioxidants react with DPPH, the stable free radical is paired off and rapidly reduced to 1,1-diphenyl-2-picryl hydrazine in the presence of a hydrogen donor. The gradation of discoloration is dependent on the strength and concentration of the antioxidants and indicates the scavenging potential of the antioxidants (Flieger and Flieger, 2020).

The assay was performed using varying concentrations of *T. roseo-alba* extracts ranging from 20-100µg along with the standard ascorbic acid. The scavenging capacities of various *T. roseo-alba* solvent extracts were concentration-dependent, as shown in Figure 21. The sample concentration required to reduce the initial concentration of DPPH by 50% (EC_{50}) was computed.

Figure 21. DPPH radical scavenging assay

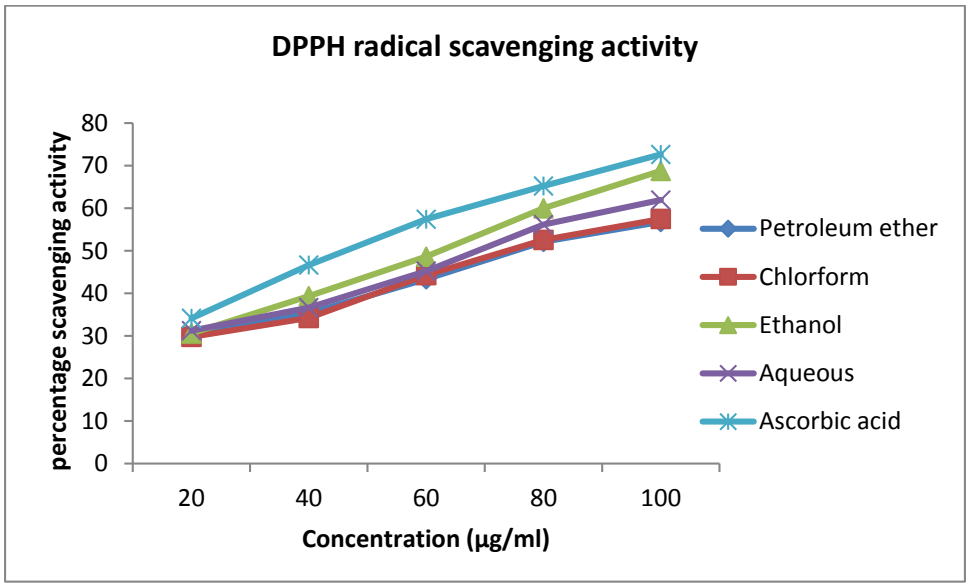

From the results, it is evident that all the extracts were able to scavenge DPPH radicals in a dose dependent manner. There was a concurrent increase in the percentage scavenging potential on the DPPH radical with increase in the concentration of all the extracts. Among the different extracts used, the ethanolic extract of *T. roseo-alba* was efficient in scavenging DPPH radicals with an EC_{50} value of 61.13µg/ml, while others exhibited moderate activity. DPPH free radical scavenging effect of different *T. roseo-alba* extracts and standards was in this order: Ascorbic acid>Ethanol >Aqueous >Petroleum ether>Chloroform. Though the ethanolic extract was able to scavenge 30 percent of the radicals at lowest concentration, the maximum activity was observed at 100µg. The results confirmed that all extracts of *T. roseo-alba* were able to scavenge the DPPH radical indicating the antioxidant potential of *T. roseo-alba* which may be due to the presence of a mixture of phytochemicals.

In line with our study, antioxidant Potential of different fractions of *Corbichonia decumbens* (FORSSK). Exell was examined by Dha and Arunprasath (2020) and highest DPPH radical scavenging activity (IC_{50}= 23.4 µg/mL) was observed in ethanol fraction. DPPH radical scavenging activity of *C. volkensii, V. lasiopus,* and *A. hockii* was assessed by Guchu *et al.* (2020) reported the remarkable dose dependent scavenging ability of the methanolic plant extracts on the DPPH radicals which may be owing to the presence of bioactive secondary metabolites like such as flavonoids, phenols,

terpenoids, and saponins. A comparative study by Ahmad *et al.* (2020) documented the efficient reduction of DPPH radical with the addition of methanolic extract of *Andrographis paniculata* which was correlated with the presence of high content of flavonoids. A study by Okoro, (2017), on *in vitro* antioxidant properties of different extracts of *Ethulia conyzoides* revealed the strongest anti-radical activity in acetone extract due to the hydrogen donating ability of the phytoconstituents in the extract.

In tune with the above cited literature, it may be inferred from the current study that, the capacity of the plant extract to scavenge DPPH radicals may be due to their hydrogen donating capacity of the antioxidant compounds present in *T. roseo- alba* and thus serving as free radical scavengers.

4.1.5.2. $ABTS^+$ radical scavenging Assay

The ABTS assay is an efficient method for evaluating the antioxidant activity of natural compounds that donate hydrogen and chain breaking antioxidants (Priyanga *et al.,* 2015). A protonated radical, $ABTS^+$ radical, has a specific absorption at 734 nm, which declines with proton radical scavenging, which is also known as an excellent peroxidase substrate frequently used to study the antioxidant properties of natural compounds (Muneeswaran *et al.,* 2020).

The decolorization of the $ABTS^+$ radical, which was detected spectrophotometrically at 734 nm, was used to quantify the extract's overall antioxidant capacity. Figure 22 indicates the ABTS radical scavenging potential of the various extracts of *T. roseo-alba* at different concentrations. The findings revealed that different extracts of *T. roseo-alba* exhibited varying degrees of $ABTS^+$ radical scavenging capacity, which was concentration dependent. From the results, it may be postulated that, the ethanolic extract of *T. roseo-alba* exhibited a higher inhibitory potential compared to other extracts with a maximum percentage inhibition of 70.41 ± 0.12 at 100 µg/mL and an EC_{50} value was found to be 55.4 µg/mL. The results were compared with the standard Vitamin C and the values evidenced the antioxidant potential of the extract.

Figure 22. ABTS^{+} radical scavenging assay

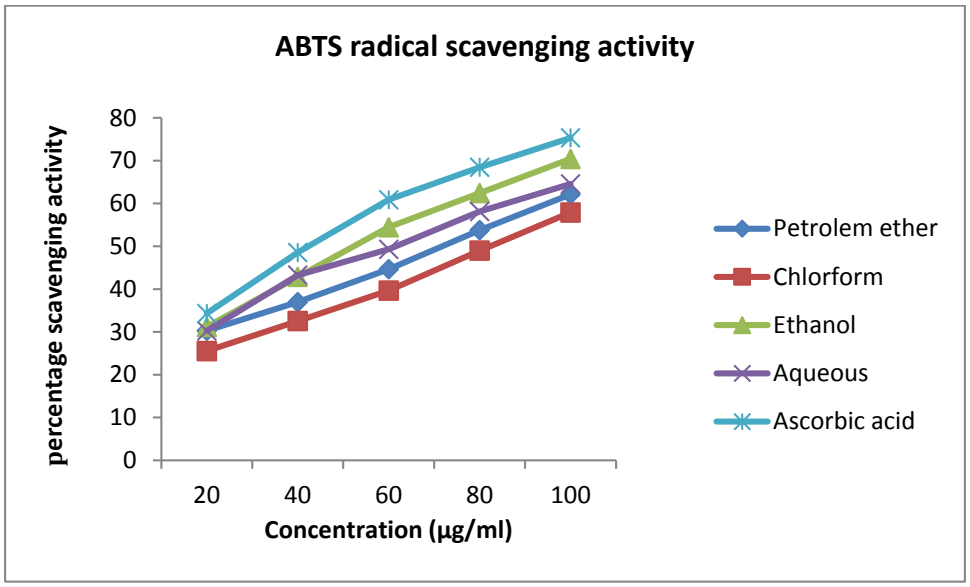

Our results are in accordance with More and Makola, (2020), who studied the ABTS radical scavenging ability of various extracts of *Solanum sisymbriifolium* leaf extracts and higher inhibitory potential was observed with ethanol extract with an EC_{50} of 39.4µg/mL which could be attributed to the existence of principle bioactive secondary metabolites that may contribute to radical scavenging activity and neutralization of ROS. A study by Muneeswaran *et al.* (2020) evaluated the ABTS radical scavenging activity of various leaf extracts of *Cassia auriculata* on radical scavenging potential of ethanolic and methanolic leaf extract were on par with the standard trolox and found to be dose dependent. Similar results were also reported by Mangoale and Afolayan, (2020) on ABTS radical scavenging potential of wild and cultivated *Alepidea amatymbica* rhizome extracts of varying polarity and they recorded dose dependent scavenging potential towards ABTS^{+} radicals by aqueous extract of wild plant extract which could be ascribed to the presence of polyphenolic compounds. Several extracts of *Schima wallichii* was assessed for its ABTS radical scavenging activity by Lalhminghlui and Jagetia, (2018) and they established the potency of the ethanol extract in reducing ABTS^{+} radicals.

The ethanolic extract of *T. roseo-alba* showed good scavenging activity towards ABTS radical which might be due to the transfer of electrons between hydrophilic compounds and ABTS radical. In line with the above cited literature, it may be concluded that the ability of *T. roseo-alba* to inhibit or quench ABTS free radicals could be ascribed to their polyphenolic compounds.

4.1.5.3. Hydroxyl radical scavenging assay

Hydroxyl radicals are considered to be the most chemically reactive species among all the oxygen-centered radicals, hence they rapidly react with biomolecules such as proteins, lipids, and nucleic acids in almost every biological membrane, eventually leading to *in vivo* cell damage. The Fenton reaction generates hydroxyl radicals in the presence of reduced transition metals such as $Fe2^{+}$ and H_2O_2 (Zhou *et al.,* 2020). The findings of hydroxyl radical scavenging potential of the plant extract and ascorbic acid are depicted in Figure 23.

Figure 23. Hydroxyl radical scavenging assay

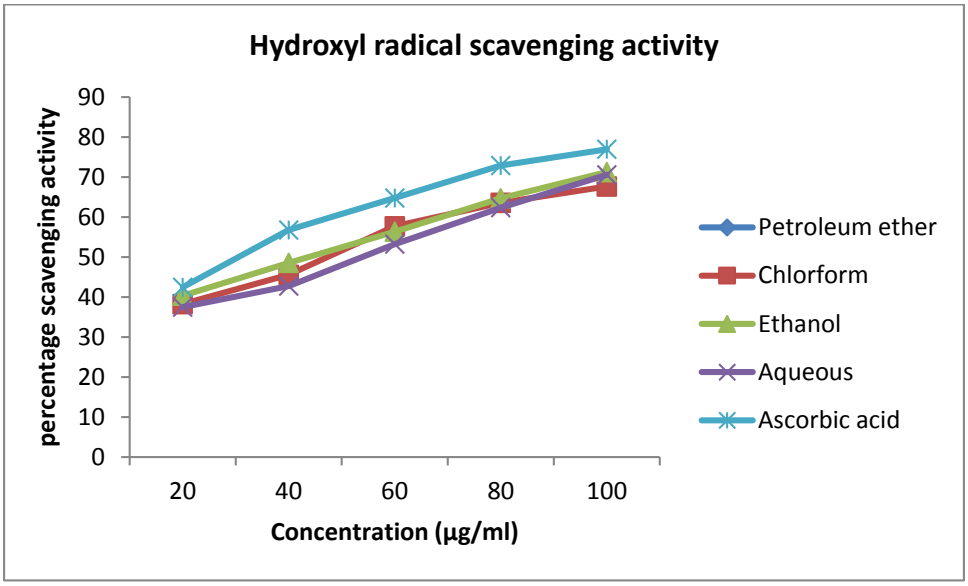

The antioxidant property of an extract or compound is directly linked with its hydroxyl radical scavenging potential, as seen by the low intensity of red colour. Hydroxyl radicals were efficiently inhibited and degradation of 2-deoxyribose was prevented by all the extracts of *T. roseo-alba* when added to the mixture. Among the various extracts tested, ethanolic extract exhibited greater antiradical activity with the maximum percentage inhibition of 71.24 at 100µg/ml with an EC_{50} value of 44.11 µg/ml while standard ascorbate was found to have 76.94 % scavenging activity at 100µg/ml, which was higher than that of all the extracts tested (Figure 23). Extracts with a lower EC_{50} value have a greater potential for free radical scavenging than extracts with a higher EC_{50} value.

In line with our study by Hasan *et al.* (2020) on antioxidant potential of different fractions *Magnolia champaca* L. (Magnoliaceae) stem bark extract recorded the high

hydroxyl radical scavenging activity of chloroform fraction with IC_{50} of 9.98 µg/ml. Current study results are in agreement with Tchimene *et al.* (2016) who have investigated the hydroxyl radical inhibiting activity of lupeol extracted from the methanol extract of *Crateva adansonii* Oliv. leaves. The study revealed that the hydroxyl radicals were effectively scavenged by the sample lupeol and thus the degradation of 2-deoxyribose was prevented. A comparative study by Zhou *et al.* (2020) on Screening of the antioxidant Potential of various extracts from *Clerodendrum cyrtophyllum* Turcz leaves shown the efficiency of *n*-butyl alcohol fraction in hydroxyl radical scavenging ability compared to other fractions and thus proving its antioxidant potential which was correlated with the high content of phenols and flavonoids in the plant. A study by Barreto *et al.* (2020) on the analysis of free radical scavenging activity from ethanolic extract of *Agave sisalana* agro-industrial residue revealed the efficient concentration-dependent hydroxyl radical scavenging ability of ethanol extract, attaining 71.38% ± 3.25 at 2.0 mg/mL.

In compliance with these cited literature, it can be inferred from the current study that the hydroxyl radicals were scavenged by the extracts of *T. roseo-alba* owing to the presence of polyphenol rich compounds, thereby preventing the generation of cellular damage caused by free radicals and thus contributing to its antioxidant potential.

4.1.5.4. Hydrogen peroxide Radical Scavenging Assay

Hydrogen peroxide is a delicate oxidizing agent which, typically via the oxidation of essential thiol (-SH) groups, directly inactivates many enzymes. In order to form hydroxyl radicals, it can probably react with Fe_2^+ and possibly Cu_2^+ ions and this may be the cause of many of its toxic effects. In addition, oxidative stress and inflammatory reactions, which are linked to pathological disorders like cancer, diabetes, and cardiovascular disease, are caused by an abnormal accumulation of H_2O_2 scavenging of hydrogen peroxide relies on the phenolic content present in the plant extract that can donate electrons to H_2O_2, thereby neutralising it into water (Aryal *et al.* 2019). The scavenging of hydrogen peroxide by the extract in a dose dependent manner is illustrated in Figure 24.

In the present study, the various extracts of *T. roseo-alba* were subjected to oxidative stress by the addition of H_2O_2. Though all the extracts of *T. roseo-alba* tested were capable of scavenging H_2O_2 to a considerable extent, ethanolic extract was found to exhibit greater antiradical activity when compared to other extracts. Maximum

scavenging activity was observed at 100 µg/ml with an EC_{50} value of 76.88 µg/ml. However, with a consistent increase in the concentration of all the extracts of *T. roseo-alba,* increased hydrogen peroxide radical scavenging activity was observed.

Figure 24. Hydrogen peroxide radical scavenging assay

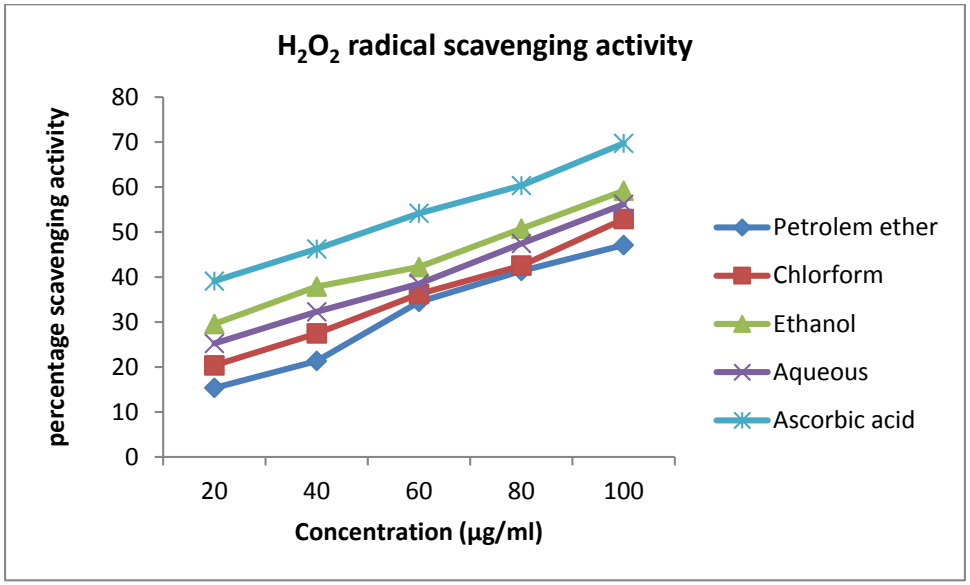

In line with our work, Gebreslassie *et al.* (2020) investigated H_2O_2 radical scavenging activity of ethyl acetate leaf extract of *Rumex nervosus*. It can be inferred from the results of the current study that the plant extract exhibited promising hydrogen peroxide radical scavenging properties with an IC_{50} value of 79.75 µg/ml. In another study, Ginting *et al.* (2020) proved the dose-dependent inhibition of hydrogen peroxide by ethanol extract of *Ficus elastica* leaves and their bioactive phytocompounds indicating its antioxidant potential. A study by Ruskin *et al*. (2017) on radical scavenging and antioxidant activities of various extracts of *C. coromandelicum* (Burm. f.) Alston. leaves with different *in vitro* assay systems revealed efficient H_2O_2 scavenging activity which was ascribed to the presence of bioactive secondary metabolites. A study by Keshari *et al.* (2018) on the assessment of antioxidant activity of medicinal plants *Withania coagulans, Cestrum nocturnum, Cymbopogon citratus and Catharanthus roseus* revealed the ability of the plants in scavenging hydroxyl radicals in a dose dependent manner owing to the presence of various bioactive metabolites such as phenols and flavonoids and thus proving their antioxidant potential.

Based on the cited literature, it can be concluded that the ability of *T. roseo-alba* extracts to scavenge H_2O_2 is due to their phenolics, which can transfer electrons to H_2O_2 and therefore neutralise it to water.

4.1.5.5. Nitric oxide scavenging assay

Nitric oxide is a free radical produced by mammalian cells that regulates neurotransmission, vascular homeostasis, antibacterial, and anticancer activity in a variety of physiological processes. Because excessive NO production is linked to a variety of diseases, it would be fascinating to create powerful and specific NO inhibitors for future therapeutic usage (Adebayo *et al.,* 2019).

In the present study, various extracts of *T. roseo-alba* leaves were assessed for their inhibitory potential against NO generation *in vitro.* All the extracts were able to inhibit nitric oxide generation in a concentration dependent manner and the results are shown in Figure 25. In comparison with other extracts, ethanolic extract was found to be effective in nitric oxide radical scavenging activity. The ethanolic extract showed maximum inhibition of 73.73 ±0.23 at a concentration of 100 µg/mL with an EC_{50} value of 35.62 µg/mL. In the present study, *T. roseo-alba* was proved to have strong nitric oxide radical scavenging activity, it competes with oxygen for nitric oxide and so prevents the formation of nitrite.

Figure 25. Nitric oxide radical scavenging assay

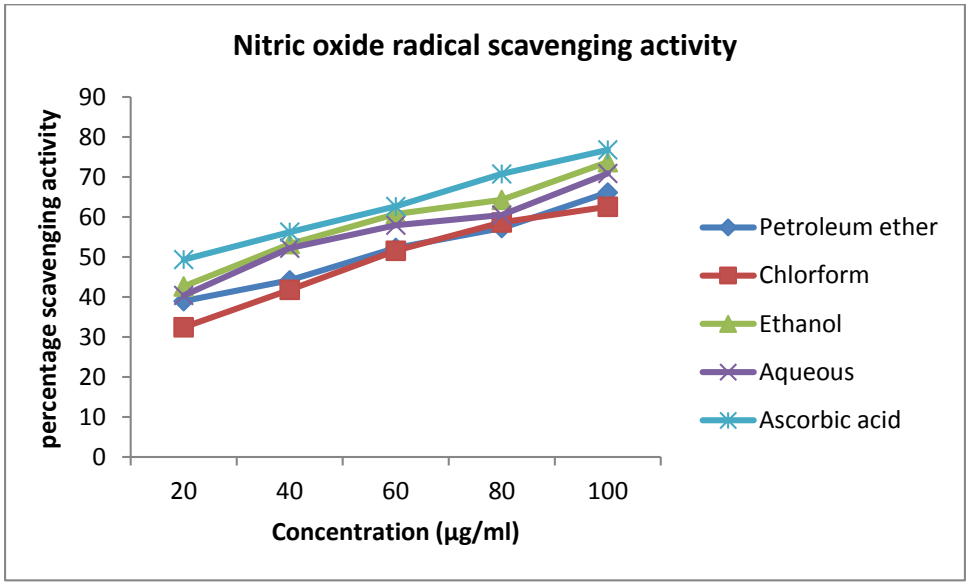

In par with our work, Borquaye *et al.* (2020) studied the nitric oxide radical scavenging potential of *Reissantia indica, Grosseria vignei* and *Cissus cornifolia* ethanolic extracts. Among them, *Reissantia indica* extract unveiled good scavenging activity with an IC_{50} of 320 ± 3.2 µg/ due to the presence of polyphenols. Our findings are also supported by Chiedozie *et al.* (2020) they documented the concentration dependent nitric oxide radical scavenging activity using *Cucurbita maxima* fruit juice which was equivalent with ascorbic acid standard. Awala and Oyetayo, (2016) evaluated Nitric oxide radical scavenging activities of different extracts of *Trametes lactinea* and revealed the efficient scavenging ability of methanolic extract which was directly linked with the presence of flavonoids which may neutralize damaging effects of free radicals. An Attempt was made by Hassan and Hassan, (2015) to establish the efficient nitric oxide scavenging ability of potato peel ethanolic extract than that of aqueous extract and positive correlation was found between the potato peel extract concentration and nitric oxide scavenging activity.

Thus in the current study, *T. roseo-alba* extracts showed substantial nitric oxide radical scavenging activity, which may be ascribed to the presence of phenols and flavonoids, which compete with oxygen for nitric oxide and so prevent nitrite formation. Therefore, the current study proved the antioxidant capacity of the study plant by inhibiting nitric oxide generation and thus may be used as natural source of antioxidants that provide protection against damage caused by free radicals.

4.1.5.6. Superoxide radical scavenging assay

Superoxide anion radical, a highly reactive free radical, causes cellular damage by indirectly triggering lipid oxidation. The superoxide ($O_2^{\bullet-}$) radicals can be broken down to produce stronger reactive oxygen species, such as hydroxyl radicals and singlet oxygen. As a result, scavenging $O_2^{\bullet-}$ could reduce the production of various other ROS and protect cells from oxidative damage (Lalremruati *et al.,* 2019). NBT is reduced by Superoxide radical to a blue coloured formazan which can be measured at 560 nm in the present analysis.

Figure 26. Superoxide radical scavenging assay

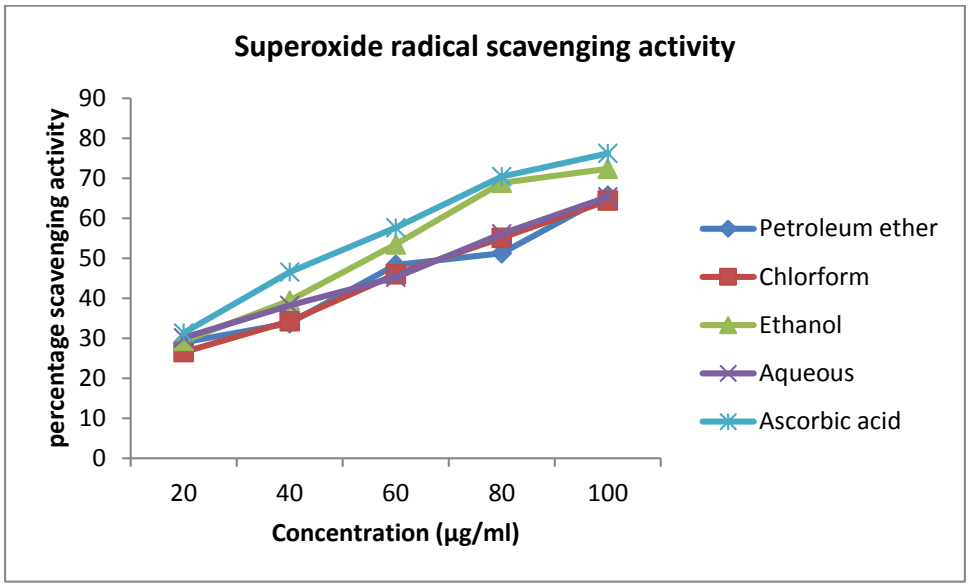

The ability to inhibit the generation of superoxide by different extracts of *T. roseo-alba* were assessed and the results are presented in Figure 26. The decrease in absorbance at 560 nm represents the free radical scavenging potential of the plant extracts against the superoxide anion in the reaction mixture. Although all the extracts were able to exhibit inhibitory activity against superoxide generation in a concentration dependent manner, the ethanolic extract of *T. roseo-alba* leaves exhibited maximum superoxide radical scavenging activity with an EC_{50} value of 55.4 µg/mL. From the results it may be suggested that the ethanolic extract of *T. roseo-alba* leaves acquire antioxidant activity by inhibiting superoxide radical generation which may be owing to the existence of bioactive metabolites in the plant.

Our observations are in line with an earlier work carried out by Adeosun *et al.* (2016) who revealed the efficacy of methanol extract of *Phoenix dactilyfera L.* seed to inhibit superoxide anion in a dose dependent manner owing to the presence of various phytochemicals. Sudhakar *et al.,* (2020) demonstrated the potency of 50% Hydroethanolic Polyherbal Crude exract of *Gymnema sylvestre*a and *Urgenia indica* in scavenging superoxide radicals. Selvaraj *et al.* (2019) made an attempt to analyze superoxide anion inhibiting potential of aqueous extract of *A. racemosus* and the results revealed the maximium inhibition against superoxide radical activity which might be due to the presence of active metabolites. In another study, Kaur and Saxena, (2020) compared

superoxide radical scavenging potential of different extracts of *Phaseolus vulgaris* and the methanolic extract showed the highest superoxide radical scavenging activity among the extracts tested.

In agreement with the above literature, the ethanolic extract of *T. roseo-alba* inhibits $O_2^{\bullet-}$ generation efficiently which might be attributed by the presence of various active metabolites mainly phenols and flavonoids and thus preventing oxidative damage.

4.1.5.7. Reducing power assay

For the assessment of antioxidant activity of polyphenolic compounds present in the plant, reducing power assay is commonly used. The ability of a chemical to transport electrons is related to its reducing power, which can be used to determine its antioxidant activity (Subramani and Nachimuthu, 2019). The reduction power of the sample can be examined by monitoring the development of Perl's Prussian blue at 700 nm (Mbaoji and Nweze, 2020). The reduction potential of various *T. roseo-alba* extracts and standards at different concentrations was examined by their capability to convert Fe_3^+ to Fe_2^+ and the results are depicted in Figure 27.

Figure 27. Reducing power assay

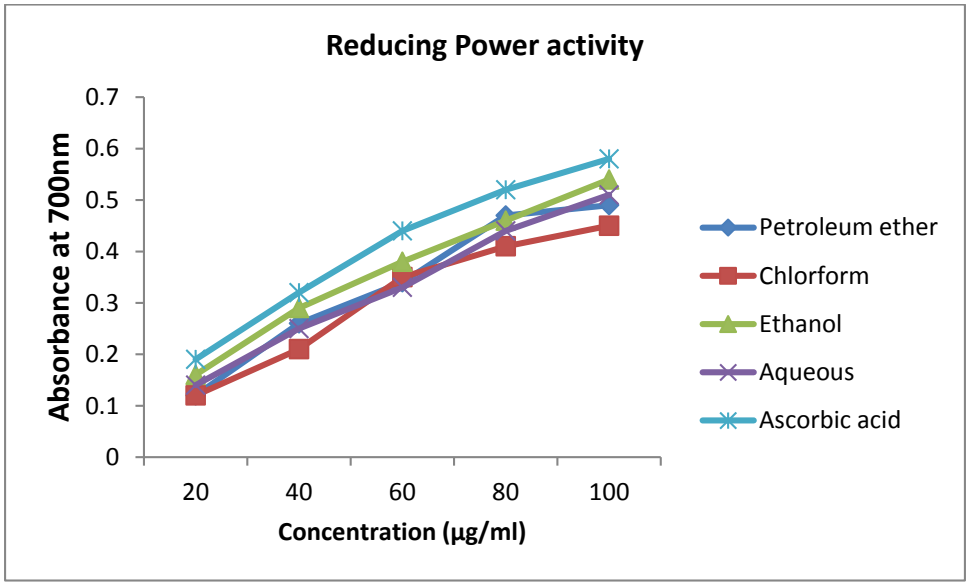

Based on the results, it is documented that there is a dose dependent rise in reducing potential of all the tested samples. Among the different extracts tested, ethanolic extract of *T. roseo-alba* was found to have higher reduction potential. Maximum reducing power activity of ethanolic extract was found at 100µg/ml signifying

their dose dependent activity which was comparable with the standard ascorbic acid**.** The ability for the reduction of Fe (III) is due to the donation of hydrogen from phenolic compounds, which is also dependent on the presence of a reducing agent. Furthermore, phenolic compounds' antioxidant activity is influenced by the amount and position of their hydroxyl groups (Gudise *et al.,* 2019). The antioxidant potential of phenols and flavonoids were owing to their redox properties, metal chelating ability and quenching of singlet oxygen (Divya and Kalaiselvi, 2017).

Similar observations were recorded by Brhane, *et al*. (2018) on the reductive capabilities of *Aloe adigratana* ethanolic gel extract. The reducing power of *Aloe adigratana* ethanolic gel extract increased with increase in concentration. The methanol and chloroform extracts of aerial parts of *Kickxia ramosissima* (Wall.) Janchn. was tested for their ability to reduce Fe^{3+} to Fe^{2+} and the results reported that the methanolic extract of *Kickxia ramosissima* unveiled strong reducing capability, which can be ascribed to bioactive components in the plant (Binish *et al.*, 2021). Batool *et al.* (2019) studied the antioxidant activity of *Brachychiton populneus* leaves using different solvents and proved the efficient reducing ability of aqueous fraction of *Brachychiton populneus* which was correlated with the Total phenol and Total flavonoid content of the plant. In agreement with our findings, Ekin *et al.* (2017) explored the potent reducing power activity of ethanolic extract of *C. meyeri* leaves than the aqueous extract which was owing to high phenolic content in the ethanolic extracts.

In accordance with these supporting studies, the findings of the present study shows that the phenolic compounds present in the candidate plant might serve as electron donor to break the free radical chain reaction thereby contributing to reducing ability of the plant.

In an attempt to analyse free radical scavenging and antioxidant potential of various solvent extracts of *T. roseo-alba,* it was observed that all the radicals tested in the present study are competently scavenged to a greater extent by the ethanolic extract of *T. roseo-alba,* which reveals the involvement of bioactive metabolites namely, phenolic compounds, flavonoids and terpenoids in the elimination of exposed radicals. It may be inferred from the results of the present study that the ethanolic extract of *T. roseo-alba,* possesses strong antioxidant potential owing to the existence of phenolic components and other active metabolites in the extract, which was confirmed by the free

radical scavenging property. The findings of the current study indicated that ethanolic extract of *T. roseo-alba* scavenges free radicals efficiently and thereby diminishing lipid peroxidation and associated cellular damage.

Phase II

Nanotechnology is a broad, interdisciplinary field of research, dealing with the production, manipulation and use of material ranging in nanometers (Yasmin *et al.,* 2020). Nanoparticles have unique physical, chemical, and biological capabilities at the nanoscale as compared to their counterparts at larger dimensions. This is due to a higher surface area to volume ratio, enhanced reactivity or stability in a chemical process, and increased mechanical strength, and these features have led to its use in a variety of applications (Ealias *et al.,* 2017). Silver, a noble metal with distinctive features such as excellent conductivity, chemical stability, catalytic activity, surface enhanced Raman scattering and antibacterial action, and increased oral bioavailability, has potential use in medicine (Ratan *et al.,* 2020).

4.2 Synthesis and Characterization of the AgNPs of *T. roseo-alba*

4.2.1 Synthesis of AgNPs of *T. roseo-alba*

On exposure to the ethanolic plant extract, silver ions are reduced to silver particles, and the change of colour from light yellow to dark brown (Figure 28), which could be due to surface plasmon resonance excitation led by the collective oscillations of the valence electrons present in the electromagnetic field of incident radiation (Mollick *et al.,* 2019). So it is evident from the visual observations that the plant extract of *T. roseo-alba was* a good reducing agent for the reduction of Ag^+ ions to Silver nanoparticles. Nahar *et al.* (2020) also reported similar results with *Cinnamomum tamala* leaf extract for the synthesis of silver nanoparticles. The formation of AgNPs using *Saccharum officinarum* stem extract is indicated by a visually observable change in the colour of the reaction solution from colourless to dark brown (Paulkumar *et al.,* 2017). Ashraf *et al.* (2020) made an attempt to synthesise *Melia* leaf extract silver nanoparticles and proved their presence by change in brown colour of the solution. Formation of AgNPs using *O. ferruginea* leaf and bark extracts was evidenced by the conversion of pale brown to dark brown color in the colloidal solution due to excitation of SPR effect. The change of colour in the reaction mixture of plant extract and $AgNO_3$ is the first visual indication of the synthesis of AgNPs, and it is linked to the difference in the surface plasmon resonance of AgNPs during the reduction of silver ions to silver nanoparticles (Hussain *et al.,* 2020).

Figure 28. Visual Characterization of AgNPs synthesized using *T. roseo-alba*

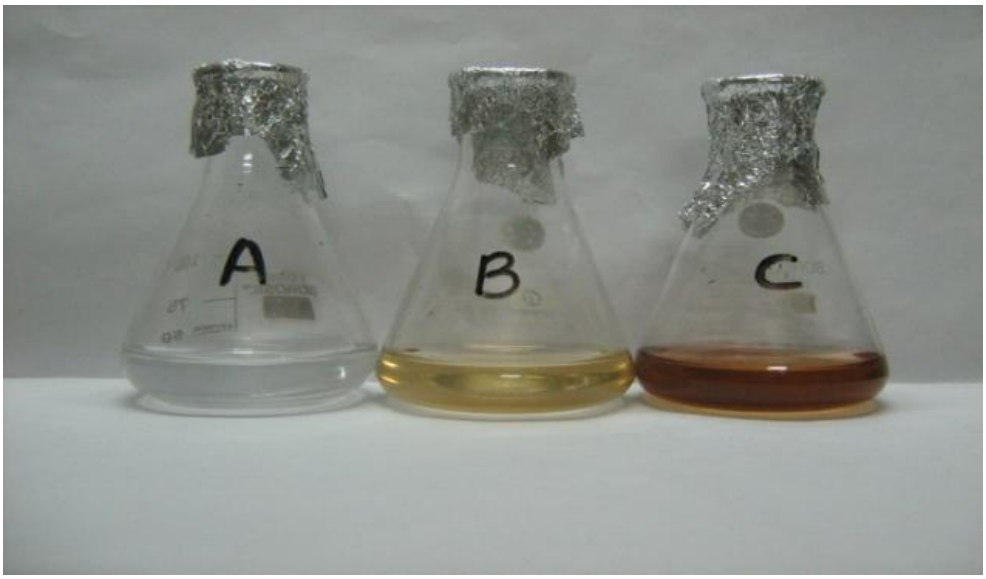

a) Aqueous extract of 1mM Silver Nitrate. b)Ethanolic extract of *T. roseo-alba.* c) Synthesized AgNPs from *T. roseo-alba*

In agreement with above reports, the candidate plant of the present study also possesses the ability to reduce Ag^{+} to Ag^{0}, which was observed by the colour change from light yellow to dark brown in the reaction mixture. The change in color is due to the excitation of Surface Plasmon Resonance and confirms the synthesis of nanoparticles.

4.2.2 Characterization of AgNPs of *T. roseo-alba*

4.2.2.1 UV-Visible Spectroscopy

The presence of various active metabolites present in the extract was identified using UV-Visible spectroscopy at the wavelength of 220 to 800 nm. The absorption spectra of ethanolic extract of *T. roseo-alba* and its AgNPs are presented in Figure 29 and 30. Distinct peaks were observed at different wavelengths indicating the presence of various phytochemical constituents and their derivatives in the sample. Also a peak at 300 nm observed clearly confirms the presence of phenolic compounds and their derivatives, which were further analyzed using High performance thin layer chromatography.

Figure 29. UV-VIS absorption spectra of ethanolic extract of *T. roseo-alba*

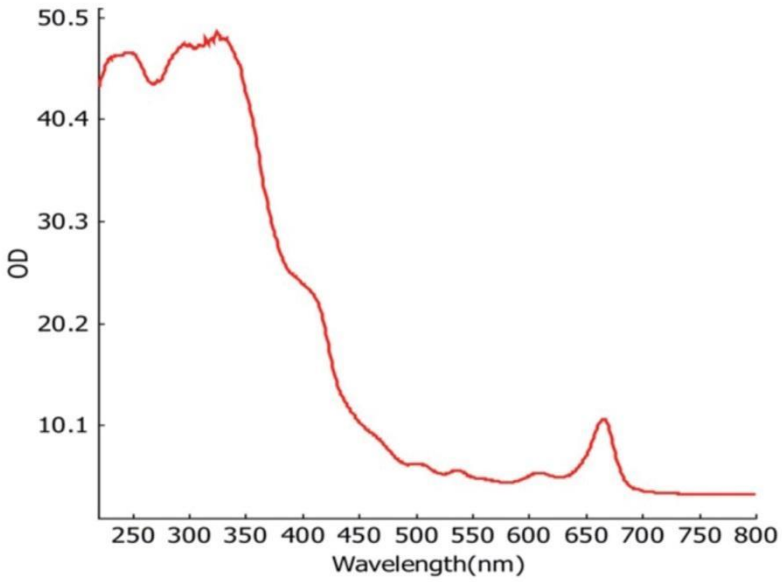

The reduction of silver ions by the plant extract and formation of silver nanoparticles was progressively observed as well as measured with UV–visible spectrometer in the wavelength range 200–700 nm. UV-vis spectroscopy is a very helpful and practical approach for monitoring AgNP synthesis and stability, as well as primary characterization of produced nanoparticles. The reduction of silver ions can be correlated with the respective UV–vis absorption spectrum which shows the surface plasmon resonance derived from the silver nanoparticles around 300-350nm. In addition, the number of absorption peaks and the breadth of SPR bands are related to the size distribution and shape of Ag-NPs in solution. Anisotropy of AgNPs is represented by several SPR bands, whereas a single band reflects primarily spherical Ag-NPs. Furthermore, according to quantum size theory, the SPR bands broaden as particle size decreases (Hussain *et al.,* 2020). The spherical shape of AgNPs was confirmed by a single SPR band recorded in our study.

Khan *et al.* (2018) recorded absorption peak at 316 nm for silver nanoparticles synthesized from leaves of *Coriandrum sativum*. The present study results are in par with Samuggam *et al.* (2021) who observed maximum intensity between the wavelengths of 300 to 400 nm for the green synthesised silver nanoparticles from ethanolic leaf extract of *Pondias mombin*. AgNPs of root extract of *Astragalus tribuloides* Delile. showed a strong surface Plasmon resonance which was centered approximately

around 430 nm (Sharifi-Rad *et al.,* 2020). AgNPs synthesized using aqueous extract of *Allium sativum* leaves by Yasmin *et al.* (2020) exhibited the typical silver plasmon absorption maxima at 400-410 nm**.** Alsubki *et al.* (2021) also reported a similar plasmon absorption maximum at 400 nm by the silver complex with AgNPs synthesized using *C. sativum* leaves.

Figure 30. UV-VIS absorption spectra of AgNPs synthesized using *T. roseo-alba*

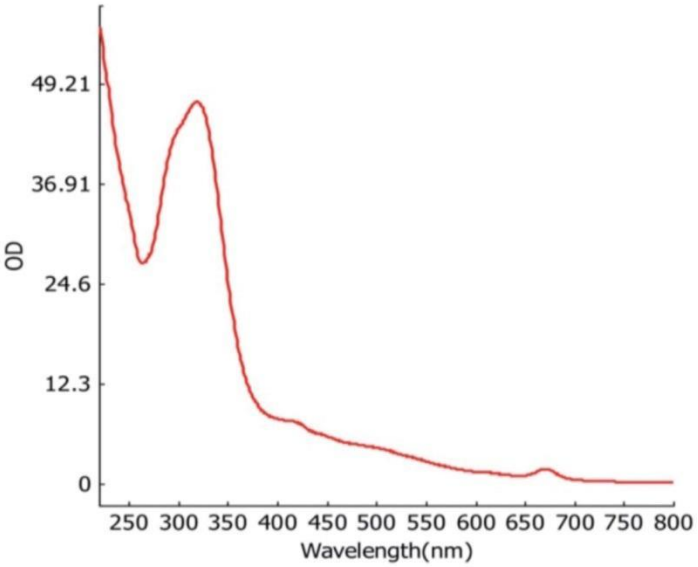

.

The results of the current study confirms the formation of spherical nanoparticles by the ethanolic extract of *T. roseo-alba* as it is evident from UV-Vis spectral peak obtained around 300-350nm. In compliance with these results, the synthesized AgNPs of ethanolic extract of *T. roseo-alba* were used for further characterization studies.

4.2.2.2 Fourier Transform Infrared spectroscopy

FTIR is a very accurate analytical technique for detecting and displaying components, chemical structure, functional groups, and molecular bonding configurations. Characterization of silver nanoparticles using FTIR is carried out to ascertain the components which are acting as coating and stabilizing agents (Jain *et al.,* 2021).

In the present study, FTIR analysis was performed out to detect the bioactive components involved in the reduction of $AgNO_3$ and to confirm their efficient stabilization. The IR spectrums of ethanolic extract of *T. roseo-alba* and its AgNPs are depicted in Figure 31 and 32.

Figure 31. FTIR spectrum of *T. roseo-alba*

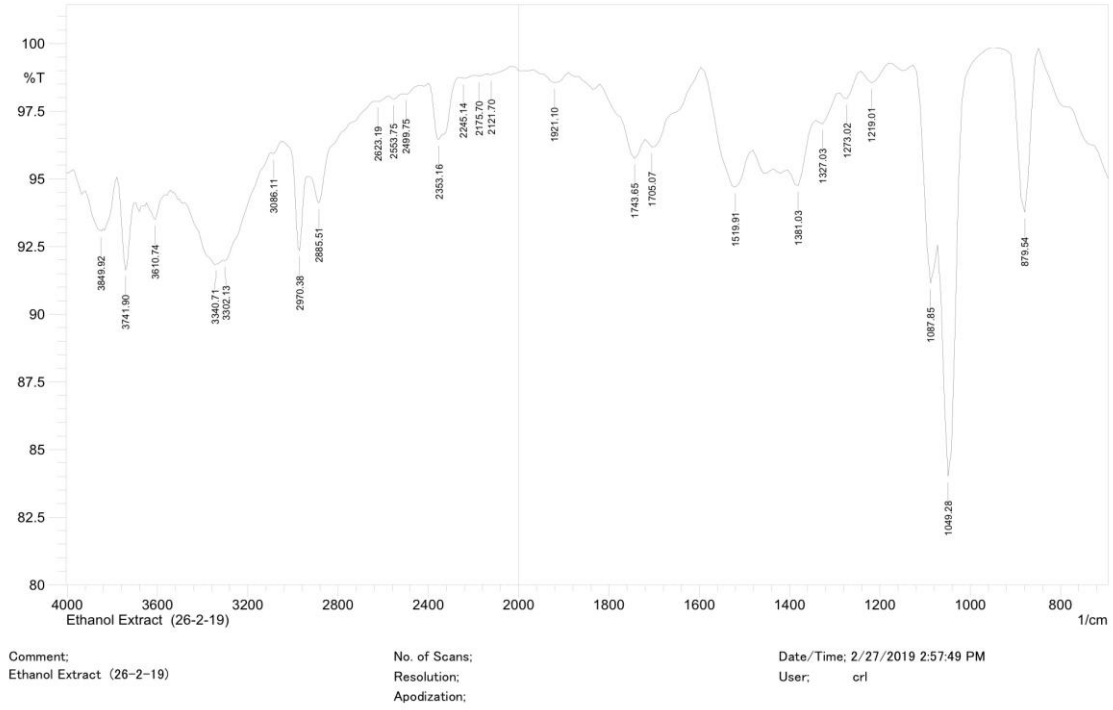

In the FTIR spectrum of ethanolic extract of *T. roseo-alba* the peaks at 3340.71cm^{-1} and 3302.13cm^{-1} corresponds to O-H vibration and stretching that implies the presence of phenolic group, peak at 2970.38cm^{-1} corresponds to C-H stretching vibration which in turn indicates the presence of alkenes, peak at 1519.91cm^{-1} corresponds to N-O asymmetric stretching vibration which reveal the presence of nitro compounds, peak at 1381.03 cm^{-1} is due to N-O stretching vibration corresponding to nitro compounds, peaks at 1273.02cm^{-1} and 1219.01cm^{-1} corresponds to C-O stretching vibration that demonstrate the existence of carboxylic acids, esters, ethers and alcohols, peaks at 1087.85cm^{-1} and 1049.28cm^{-1} corresponds to C-N stretching vibration revealing the presence of aliphatic amines, peak at 879.54cm^{-1} corresponds to N-H stretching vibration revealing the presence of primary and secondary amines.

Figure 32. FTIR spectrums of AgNPs synthesized using *T. roseo-alba*

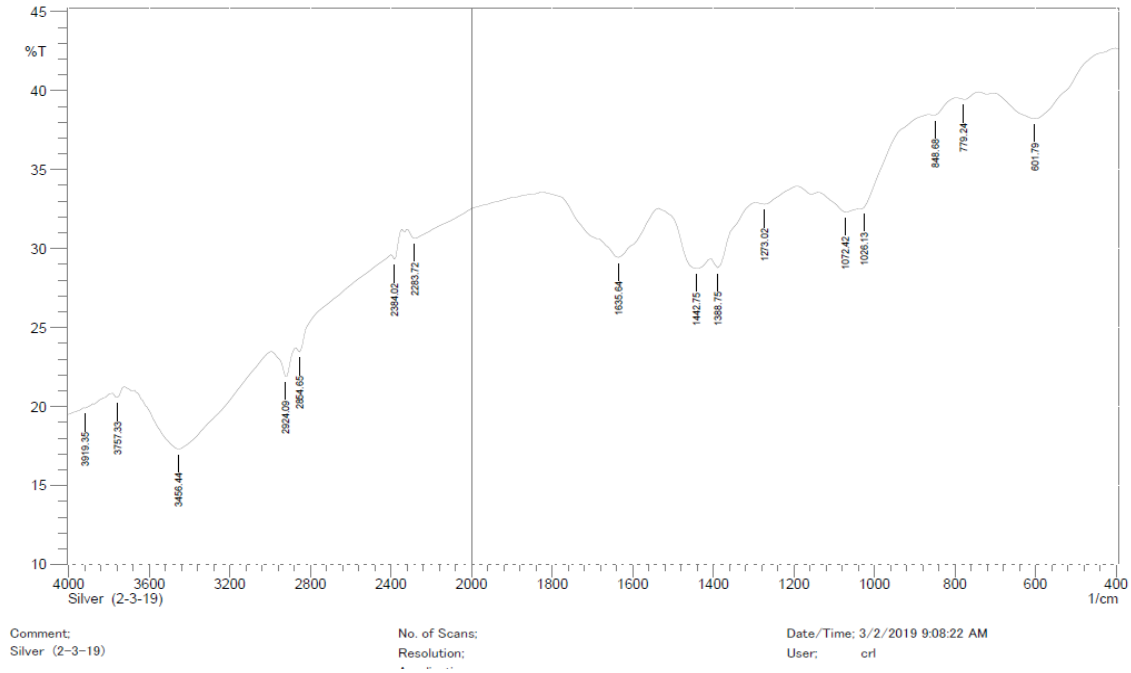

The FTIR spectra of green synthesized silver nanoparticles showed shift in many peaks that might be due to the involvement of phytochemicals in metallic nanoparticle synthesis and there was a vast shift at peak 3340.71cm^{-1} to a higher wavelength this suggest that the hydroxyl groups of phenolic compounds play a considerate role in capping of nanoparticles (Ramesh *et al.*, 2018). The shift of peak 2970.38 cm^{-1} to a lower wavelength implies that triterpenoids and saponins also have a role in nanoparticle synthesis (Hemlata *et al.,* 2020).

The potential role of bioactive compounds such as flavonoids, phenols, alkaloids, and tannins in the extracts of *T. roseo-alba* favoured the biosynthesis of nanoparticles. The absence of several basic groups and peaks of lower intensity can be seen in the IR spectra of AgNPs compared to IR spectrum of ethanolic extract which may be because of the involvement of functional groups of the phytoconstituents in the leaf extract of *T. roseo-alba* in the reduction of silver ions.

In accordance with our findings, Asomie *et al.* (2021) stated that most of the functional groups present in *Spondias mombin* extract exhibited a crucial role in the biosynthesis of silver nanoparticles. He *et al.* (2017) unveiled green synthesis of silver nanoparticles by the proteins or flavonoids present in the *Alpinia katsumadai* seed extract and consequent capping and stabilization of the synthesized AgNPs by functional

groups of proteins or carbonyl groups of flavonoids. The results obtained from the study by Vasyliev *et al.* (2020) also proved the involvement of phytoconstituents in the black currant and apricot pomace extracts in the formation and stabilization of silver nanoparticles. The participation of bioactive compounds of the *Salvia spinosa* plant in the bioreduction of silver ions into silver nanoparticles was demonstrated with variation of peaks in the IR spectrum by Pirtarighat *et al.* (2019). In the biogenic synthesis of AgNPs using *Eriobotyra japonica* (Thunb.) leaf extract, Yu *et al.* (2019) confirmed the involvement of N-H and carbonyl functional groups in the synthesis of silver nanoparticles. Studies by Hamouda *et al.* (2019) have confirmed the interactions between the chemical functional groups of active metabolites present in *Oscillatoria limnetica* and its AgNPs. The study also proved the stronger metal binding ability of the carbonyl group of amino acids and proteins which could form a layer over the metal nanoparticles to prevent clustering and thereby stabilizing the medium.

From FTIR results, it is evident that many of the active metabolites present in the plant extract form a strong coating on the nanoparticles**.** Further the bioactive molecules present in *T. roseo-alba* leaves performed a major role in the synthesis and their subsequent stabilization of silver nanoparticles in the aqueous medium. To conclude, bioreduction of silver ions by these functional groups has been confirmed and they may play a significant role in the green synthesis of AgNPs.

4.2.2.3 Dynamic Light Scattering

DLS estimates the size of AgNPs by determining the diameter of particles scattered in the colloidal suspension. DLS is based on the concept of light scattering and it is a method for characterising green synthesised AgNPs using phytoconstituents (Gurunathan *et al.,* 2018)**.** The Poly Dispersity Index (PDI) scale is dimensionless, with a value of "0″ representing the maximum level of monodispersity and a value of "1″ representing a polydisperse particle distribution (Khorrami *et al.,* 2019).

The DLS pattern of the present study reveals that the silver nanoparticles synthesized from *T. roseo-alba* have a zeta average diameter of 81.04 d.nm with (PDI) of 0.224 (Figure 33). The size of the nanoparticle measured from DLS is considerably bigger as compared to TEM measurements because the DLS method deals with the hydrodynamic radius which includes diameter of the particle and ions or molecules associated with the surface (Erjaee *et al.,* 2017). The hydration layer on the surface of AgNPs is included in the hydrodynamic size, which is often bigger than the size

estimated from scanning electron microscopy images. The bioactive constituents present in the leaf extract may also perform a role in the hydrodynamic size. For cell uptake, nanoparticle sizes of less than 150 nm and PDI values of less than 0.3 are sufficient (Cervantes *et al.,* 2019). Hence, the size and PDI value attained in the present study revealed the targeting ability of the green synthesized nanoparticles of *T. roseo-alba* leaves to specific sites and extend the period of drug activity.

Figure 33. DLS image showing the size of the AgNPs synthesized using *T. roseo-alba*

			Size (d.nm):	% Intensity:	St Dev (d.n...
Z-Average (d.nm):	81.04	Peak 1:	104.6	100.0	48.33
PdI:	0.224	Peak 2:	0.000	0.0	0.000
Intercept:	0.882	Peak 3:	0.000	0.0	0.000
Result quality :	Good				

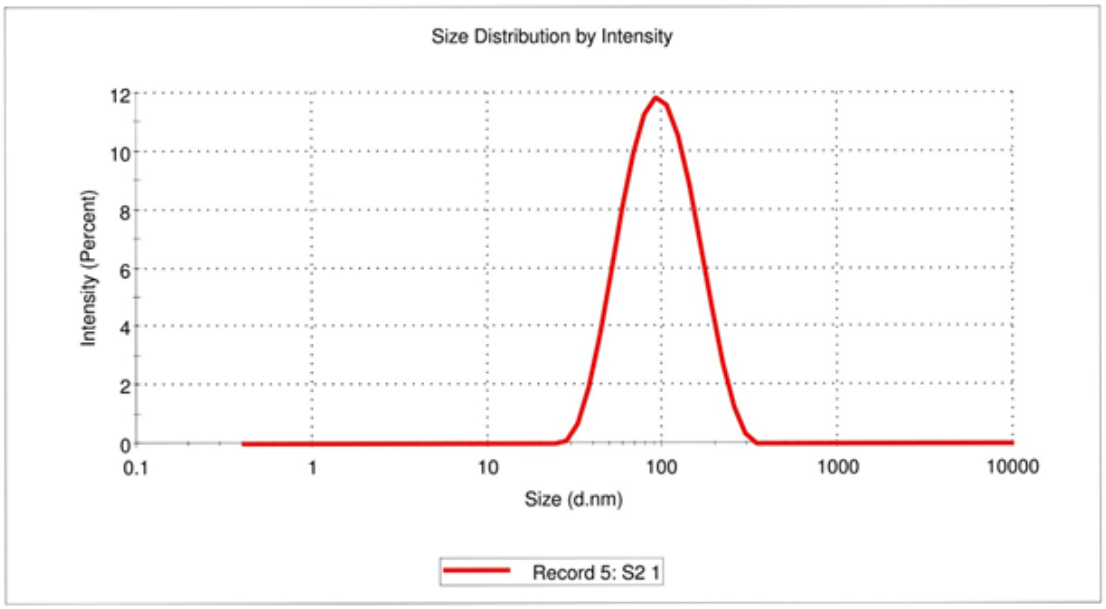

The uniformly distributed AgNPs with the average particle size (z-average) of AgNPs is ~21.29 nm were produced using *Abelmoschus esculentus* (L.) pulp extract. Since the particle size is assessed at the dried condition of the sample, TEM analysis provides an accurate size of the nanoparticles, whereas the diameter calculated using DLS is a hydrodynamic diameter (hydrated state). The hydrodynamic volume of the synthesised nanoparticles has a higher volume owing to the solvent effect in the hydrated condition (Mollick *et al.,* 2019). Subha *et al.* (2018) documented the average particle size (z-average) of AgNPs of aqueous extract of *Ipomoea pes-caprae* as 116 nm

with Polydispersity index value 0.264. The average particle size of *Pterocarpus marsupium* silver nanoparticles was measured as 148.5 nm with PDI value 0.336 (Bagyalakshmi and Haritha, 2017). The existence of average particle size silver nanoparticles from 4 to 60 nm were observed by Bhatnagar *et al.* (2019) using extracellular pigment from *Talaromyces purpurogenus*. The size distribution histogram of silver nanoparticles synthesized using aqueous leaf extract of *Azadirachta indica* indicated the average size of 34 nm (Ahmed *et al.,* 2016). The dynamic light scattering (DLS) data of the *Oscillatoria* sp. extract represented the particle size of synthesized nanoparticles as 558.1 nm with a polydispersity index of 0.580 (Adebayo-Tayo *et al.,*2019).

From the results it may be inferred that, the zeta average diameter of the synthesised nanoparticles using *T. roseo-alba* was 81.04 d.nm and this smaller size might enhance targeting efficiency of the drug to extend its activity for a longer period of time. Further studies need to be carried out to measure the efficacy of the nanoparticles under *in vivo* conditions to ensure targeted delivery of the drugs for the specified disease.

4.2.2.4 Zeta-Potential

The surface charge and stability of the nanoparticles are determined using zeta potential analysis. The velocity of the nano particles is measured under the influence of the electric field in order to assess the stability (Quintero-Quiroz *et al.,* 2019). Colloidal dispersions are stable when the zeta potential falls in the range between (larger than +30mV and lesser than - 30mV) in the absence of steric stabilisation (Pourhossein *et al.,* 2019).

The zeta potential of the AgNPs of *T. roseo-alba* was found to be -24.7 mV (Figure 34). The negative potential value of AgNPs value may be owing to the possible coating of biofunctional constituents present in the plant extract. All suspended particles with a high negative or positive potential appear to resist one another and have no tendency to flocculate, promoting long-term stability, strong colloidal character, and high AgNP dispersity.

A large negative or positive zeta potential of all suspended particles implies that they appear to repel each other and that there is no propensity to flocculate, thus promoting long-term stability, strong colloidal character, and high AgNP dispersity. A low negative or positive value of this value, on the other hand, indicates that the particles are prone to flocculation (Syafiuddin *et al.,* 2017). In the current study, from the high negative zeta potential value, it is evident that there is repulsion among the silver nanoparticles of *T. roseo-alba* and that confirmed the stability of the particles. The high

negative potential is associated with high stability, high colloidal quality, and good dispersion of AgNPs as a result of electrostatic repulsion (Alahmad *et al.,* 2021).

Figure 34. Zeta potential analysis of AgNPs synthesized using *T. roseo-alba*

			Mean (mV)	Area (%)	St Dev (mV)
Zeta Potential (mV):	-24.7	Peak 1:	-24.7	100.0	4.91
Zeta Deviation (mV):	4.91	Peak 2:	0.00	0.0	0.00
Conductivity (mS/cm):	0.378	Peak 3:	0.00	0.0	0.00
Result quality :	Good				

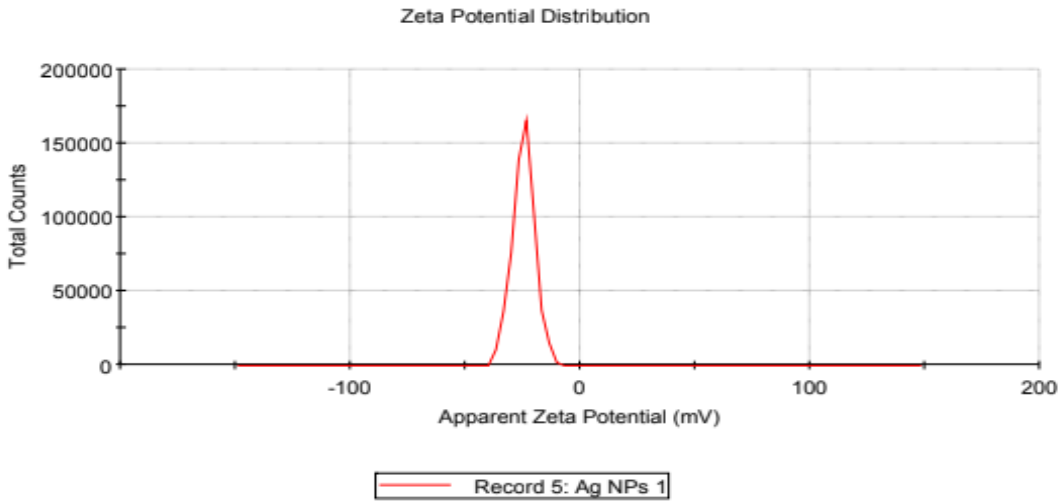

Similar findings were observed by (Murugesan *et al.,* 2019) who reported the production of silver nanoparticles using curcumin derivative with zeta potential measurement of −35.3 mV, indicating the formation of stable nanoparticles. The zeta potential value of AgNPs of *Sargassum tenerrimum* was about −39.6 mV (Khorrami *et al.,* 2019). Zeta potential measurements of green synthesised AgNPs using aqueous leaf extract of *Cucumis prophetarum* was found to be −36.7 mV suggesting the colloidal stability of the AgNPs (Hemlata *et al.,* 2020)**.** The zeta potential of silver nanoparticles of *Pueraria tuberosa* tuber was found to be -30.14 ± 2.08mV (Satpathy *et al.,* 2018). Similar to our studies, Bagyalakshmi and Haritha, (2017) documented the high stability of *Pterocarpus marsupium* silver nanoparticles, with **-**28 mV zeta potential value.

From the results of the current study, it may be inferred that the high negative potential obtained in the DLS analysis confirmed greater stability of green synthesized nanoparticles.

4.2.2.5 X-RAY Diffraction analysis

XRD is one of the most widely used techniques for characterizing NPs, and it offers the data on crystalline structure, phase nature, lattice parameters, and crystalline grain size (Mourdikoudis *et al.,* 2018). It has been carried out for the verification of phase formation of the biosynthesized silver nanoparticles and the recorded X-ray diffraction pattern was shown in Figure 35. The diffraction peaks observed at the 2θ positions of 38.15^0, 44.34^0, 64.50^0 and 77.48^0 confirms the bragg reflections corresponds to (111), (200), (220) and (311) planes and reveals the face centered cubical phase formation of the prepared silver nanoparticles [JCPDS Card No; 03-065-2871].

Figure 35. X-ray diffraction spectrum of AgNPs synthesized by *T. roseo-alba*

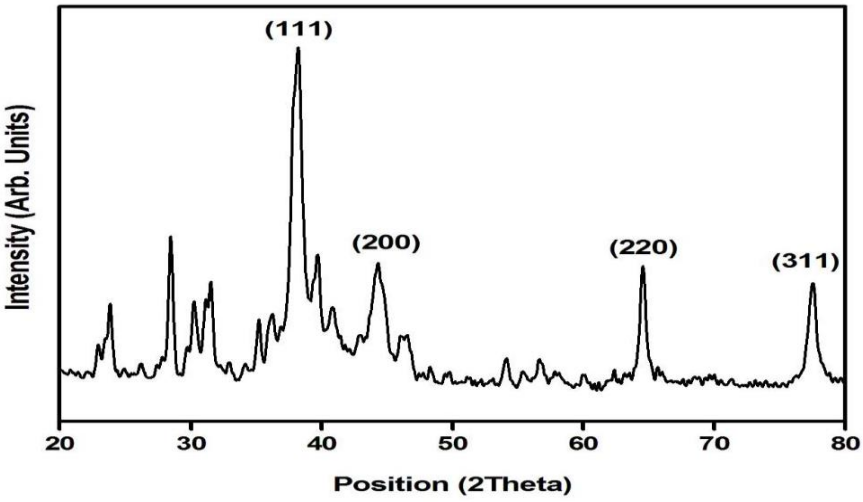

The average crystallite size calculated with respect to major intensity peak corresponds to the (111) plane and it was found to be around 27 nm which is in quite agreement with the reports on green synthesis of silver nanoparticles. Along with diffraction planes related to cubical phase formation of silver nanoparticles, quite many numbers of minor reflections were also noted from the powder X-ray diffraction studies. While comparing the phases of such impurity peaks reveals the traces of $AgNO_3$ which is the main ingredient used for the preparation of silver nanoparticles. As the sample was prepared by following green synthesis methodology using plant extract without any more coarse draining of the sample with heat treatment, it will be difficult to totally eradicate the impurity phases. Hence from the powder X-ray diffraction studies, the cubical phase formation of silver nanoparticles was identified.

These results are also in line with the results available in the literature on biosynthesis of AgNPs using plants. The XRD pattern of AgNPs synthesis using *Piper chaba* stem extracts recorded five different diffraction peaks at 2θ values of 32.12°, 38.02°, 46.1°, 64.16°, and 75.36°, which can be assigned to the lattices (101), (111), (200), (220), and (311), respectively, reveals the face-centered cubic structures ((Mahiuddin *et al.,* 2020). The XRD pattern of AgNPs of *Astragalus tribuloides* Delile. root extract shown a crystalline silver centered cubic structure based on the main diffraction peaks observed at the 2Ɵ values of 38.6^0, 46.4^0, 64.8^0, 77.9^0 and 82.3^0, which corresponded to the (111), (200), (220), (311), and (222) with the particle size of 34.2 nm (Sharifi-Rad *et al.,* 2020). XRD pattern of the ethanolic fruit extract of *Santalum album* silver nanoparticles revealed the Braggs reflections at 2θ values of 38.2901, 44.5583, 64.8185 and 77.4383 showed the presence of (111), (200), (220) and (311) sets of lattice plane (Mehta *et al.,* 2017). The X-ray diffraction pattern of AgNPs synthesised from *Annona muricata* showed sharp 2θ peaks at 38.13°, 44.21°, 64.47° and 77.37° corresponding to the miller indices planes (111), (200), (220) and (311) respectively and they were confirmed to be Face-Centered Cubic (FCC) crystals (Meenakshisundaram *et al.,* 2020).

Thus it can be concluded from the XRD results of the present study that the XRD diffraction pattern of the green synthesised *T. roseo-alba* confirms the face centred cubical phase formation of AgNPs.

4.2.2.6. Energy Dispersive Spectroscopy

EDX, which involves X-ray interaction with the sample, is used to assess the elemental composition, relative abundance, and contaminants of nanoparticles. Existence of silver crystallites was proved by the presence of emission peaks at 3 keV and the impurity-free nature of AgNPs also determined by observing the absence of any other peaks. The metabolite interaction with AgNPs on the surface is represented by the presence of other peaks such as carbon and oxygen (Radhakrishnan *et al.,* 2018).

Figure 36 shows the EDX image of AgNPs Synthesized from ethanolic extract of *T. roseo-alba*. The results clearly indicate silver nanoparticles of *T. roseo-alba* displayed an intense signal at 3 KeV, which is considered to be characteristic for metallic silver nanoparticles due to surface plasmon resonance. The EDAX analysis confirmed the weight percentage of silver as 48.34 obtained by using *T. roseo-alba*. Other weak signals with characteristic absorption for copper and carbon may be owing to the

existence of organic compounds present in the ethanolic plant extract, which represent the capping of phytosynthesized AgNPs by the biomolecules present in the plant.

The EDS signals of AgNPs produced by *Myrtus communis* L. extract confirmed the presence of silver particles which was evident from the optical absorption peak at 3KeV ((Abuderman *et al.,* 2019). In agreement with our work, similar findings were also observed by Singh *et al.* (2019), they recorded a sharp spectral signal in the silver region at 3.5 keV for silver nanoparticles of *P. integrifolia* leaf extract. The elemental composition of the silver particles synthesized using aqueous leaf extract of pomegranate extract was studied by (Sarkar and Kotteeswaran, 2018) and they revealed strong signals in the silver region around 3.2 keV with atomic weight percentage as 0.55. The EDX profile of the AgNPs from *Volkameria inermis* extract revealed the presence of typical peaks for silver (Krishnadhas *et al.,* 2017). The characterization of AgNPs synthesized using ethanolic *Coccinia indica* leaf extract demonstrated the physically powerful signals for Ag atoms and also the EDX pattern clearly showed the crystalline nature of AgNPs (Chinni *et al.,* 2021)**.** The elemental composition of AgNPs synthesized using Terrestrial fern with an intense signal for Ag at 3.0 keV was confirmed by Femi-Adepoju *et al*. (2019).

Figure 36. Energy dispersive X-ray spectrum of AgNPs synthesized using *T. roseo-alba*

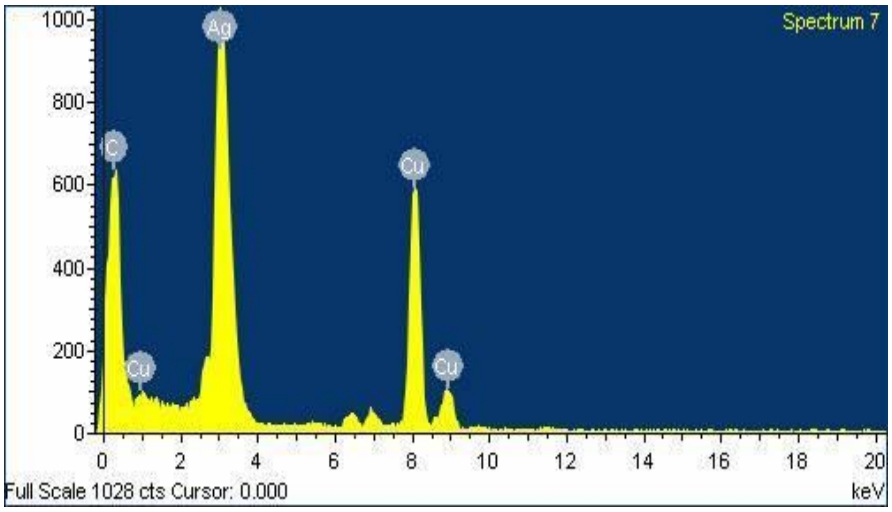

Element	Weight%	Atomic%
C K	7.27	34.55
Cu K	44.39	39.87
Ag L	48.34	25.58
Totals	100.00	

The current study outcomes are in agreement with the above cited literatures and it can be inferred that the candidate plant extract was able to support the nanoparticles formation with weight percentage of silver as 48.34.

4.2.2.7. Scanning electron microscope

SEM was used to attain a better insight into the morphology and size of the silver nanoparticles. When an electron is reflected from the sample's surface, an image is generated. From the data obtained from high-resolution images of the surface of nanoparticles, important attributes like size, shape, topography, composition, electrical conductivity can be studied (Jain *et al.,* 2021). The results of the study showed that the diameter of the silver nanoparticle of *T. roseo-alba* was about 5-100nm and they were spherical in shape as shown in Figure 37.

Figure 37. Scanning electron microscopic image of AgNPs synthesized using *T. roseo-alba*

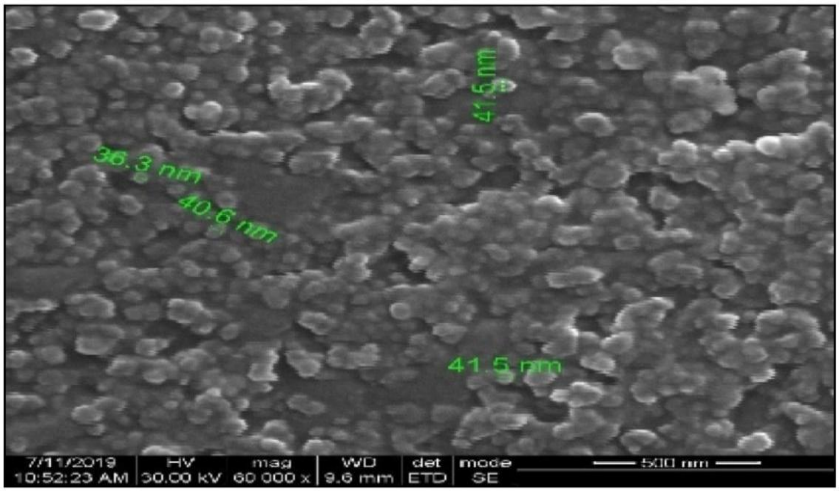

Similar patterns of SEM micrographs of silver nanoparticles synthesised using extract of *Anthemis atropatana* were also reported by Dehghanizade *et al*. (2018) with the size of about 10–80nm with mean size of 38.8nm. Monodispersed spherical silver nanoparticles of varying sizes with low agglomeration were produced by using alkalinized *Cymbopogon citratus* leaf extract (Ajayi and Afolayan, 2017). A study carried out by Yadav and Mendhulkar, (2018) demonstrated the presence of uniform and spherical shape of AgNPs synthesised by leaf extract of *Camellia sinensis* in the range of 13- 30 nm in size. The FESEM micrographs revealed the synthesis of predominantly

crystalline well dispersed AgNPs with varying sizes using the spice blend extract consisting of garlic, ginger and cayenne pepper (Otunola and Afolayan, 2018)**.**

From the findings of the current study, it can be inferred that the spherical shaped particles of varying sizes have been observed from the SEM Micrographs.

4.2.2.8. Transmission electron microscope and SEAD

TEM uses a beam of electrons to interact with the ultra thin sample and gives the most precise and high-resolution imaging data on the morphology and dispersion of nanoparticles at nanometer resolution (Mourdikoudis *et al.,* 2018). Selected Area Electron Diffraction (SAED) is a technique carried out along with TEM for the characterization of the crystallinity, and lattice parameters of nanoparticles and it also validates XRD results (Gupta *et al.,* 2019).

The TEM images of the silver nanoparticles synthesized using *T. roseo-alba* at 5, 50 and 100 nm scales are shown in Figure 38. The TEM micrographs of green synthesized AgNPs revealed that they are spherical in nature and it also suggested that the size of the particles were ranging between 5-100nm.

Figure 38. TEM image of silver nanoparticle synthesized usig *T. roseo-alba* at 5nm, 50nm and 100nm

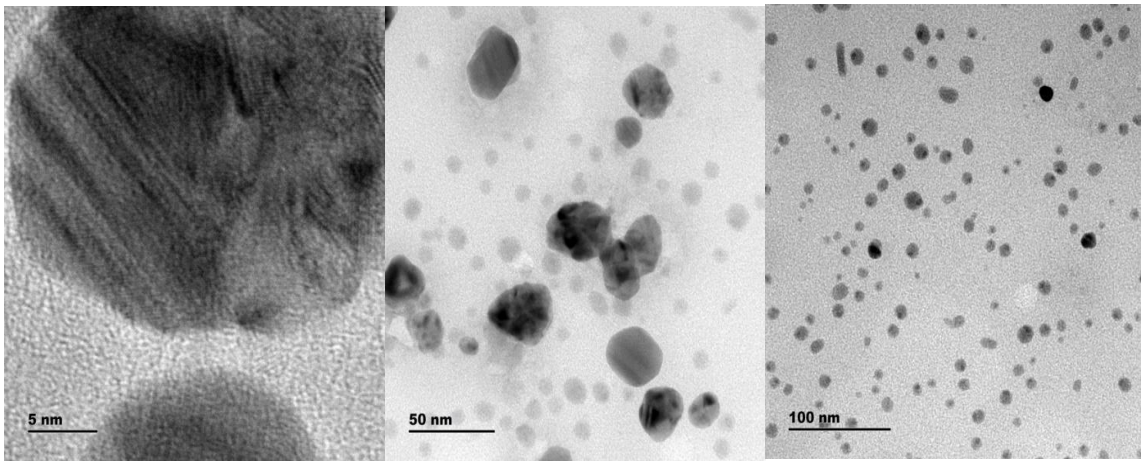

The silver nanoparticles of *T. roseo-alba* are crystalline in nature, as evidenced by the selected region diffraction pattern documented from one of the silver nanoparticles in the aggregate, which validates the results obtained from X-ray diffraction data. As seen in Figure 39, SAED spots indicate different crystallographic planes of elemental silver's face centred cubic (fcc) structure.

Figure 39. Selected area electron diffraction pattern of elemental silver.

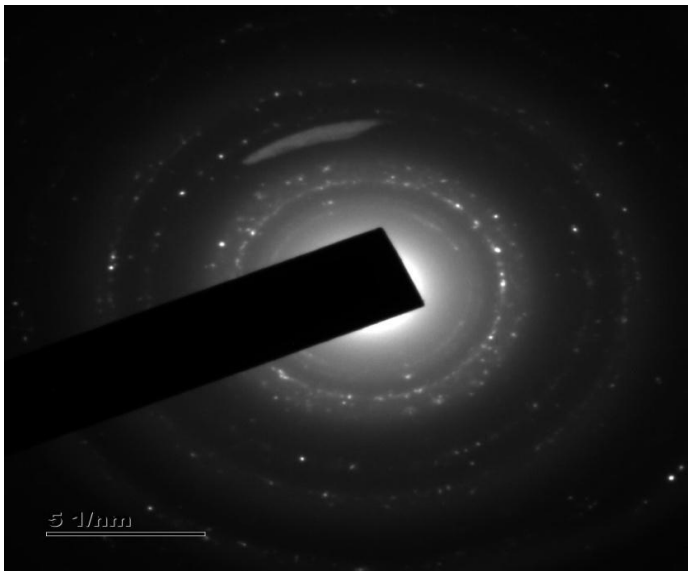

Similar results were obtained by (Lakkim *et al.,* 2020)**,** who observed spherical shape silver nanoparticles using *C. roseus* leaf extract with varying sizes and the average size of the particle was found to be 30 nm. Arshadi, (2017) demonstrated the synthesis of spherical shape nanoparticles with the average particle size of 13.24±8.591 nm using Fructose. Raj *et al.* (2018) recorded the crystalline nature of *Enicostemma axillare* silver nanoparticles using TEM Analysis. Kumar *et al.* (2017) observed spherical nature of silver nanoparticles synthesized using extracts of Andean blackberry fruit from the selected area diffraction pattern and average diameter of spherical AgNPs was found to be between 12–50 nm. The green synthesized AgNPs using *Tectona grandis* seeds extract documented the size of nanoparticles in the range between 10–30 nm and the SAED pattern validated the face-centered cubic (fcc) crystalline formation of metallic silver (Rautela *et al.,* 2019). The TEM analysis of AgNPs of *O. gratissimum* leaf extract revealed the existence of triangular shaped nanoparticles with mean particle size of 16 ± 2 nm (Das *et al.,* 2017). TEM image of the NPs synthesized from extract of *Crocus mathewii* revealed the polydispersity with average particles of 7.5 nm (2.5-25 nm) (Yildiztekin *et al.,* 2017)**.** TEM analysis of nanoparticles synthesized from leaf and root extracts of *Ricinus communis* confirmed the spherical morphology with the mean size 29 nm for nanoparticles of root and 38 nm for leaf nanoparticles (Gul *et al.,* 2021).

From the findings of the TEM analysis, the formation of spherical, crystalline, polydispersed AgNPs of varying size in the range between 5-100 nm were observed and they were coated and stabilised by the active metabolites present in the plant extract.

In conclusion, eco-friendly, cost effective green synthesis of silver nanoparticles was explored in the present study. Reduction of silver ions by the bioactive constituents in the ethanolic extract of *T. roseo-alba* was confirmed by observing the plasmon resonance between 300-350 nm using UV-Visible spectroscopy. The involvement of various functional groups in the formation and stabilization of silver nanoparticles was further validated by performing FTIR analysis. The crystalline nature of AgNPs was confirmed based on XRD pattern and high negative potential observed in the DLS analysis ensured adequate repulsion among the particles and greater stability of green synthesized nanoparticles. Morphological assessment by SEM and TEM revealed the size distribution of the particles in the range between 5-100 nm. Thus, it can be inferred that the green synthesised particles of *T. roseo-alba* adhere to the characteristics possessed by the nanoparticles. The application aspects of the synthesised nanoparticles are discussed in the following phase of the study.

Phase III

4.3 Evaluation of Anticancer potential and *in vitro* cytotoxicity of ethanolic extract of *T. roseo-alba* and its biosynthesized AgNPs

Cancer, a life threatening disease, is characterized by unrestrained proliferation of the cell and it is considered to be the main cause of death worldwide (Roshni *et al.,* 2018). Apoptosis dysfunction is a ubiquitous phenomenon in many types of cancer, and its promotion by chemical agents has been demonstrated to be a prominent strategy in cancer therapy. Using a crucial intracellular machinery of death proteases known as caspases, two distinct signalling pathways induce apoptosis. Caspases are activated in the extrinsic pathway by cell-surface death ligands released by immune effector cells. Bcl2-protein family members, such as the proapoptotic Bax, Bak, the antiapoptotic Bcl2, and Bcl XL, trigger caspases via intrinsic apoptotic pathway, resulting in extreme cellular injury. Hence, development in anticancer agents that target these molecules is considered as a promising method in cancer treatment (Pei *et al.,* 2019).

The emergence of nanomedicine as a novel and promising alternative technology has numerous advantages over traditional cancer medicines, and provides new avenues for early detection, improved treatment, and diagnosis of cancer (Bor *et al.,* 2019). The use of nanoparticles in cancer therapy has developed a novel arena of research known as nano oncology. When compared to traditional anti-cancer drugs, biogenic AgNPs have been explored in the field of nano oncology to deliver a

targeted therapy which is believed to prevent undesirable effects (Chugh *et al.,* 2018). Thus in the present study, cytotoxicity, antiproliferation and caspase mediated apoptotic effects of ethanolic extract of *T. roseo-alba* and its AgNPs were monitored through various *in vitro* analysis.

4.3.1 Cytotoxic effect of the ethanolic extract and AgNPs of *T. roseo- alba* by MTT assay

The MTT assay is a quantitative assay for the measurement of cell existence, and cell propagation. MTT is cleaved by the mitochondrial enzyme dehydrogenase in living cells, producing the purple substance formazan, which can be measured. The formazan product formation by the live cells can be correlated directly with the number of viable cells and the extent of cytotoxicity (Prajapati *et al.,* 2018).

The cytotoxic effect of the ethanolic extract of *T. roseo-alba* and its AgNPs in Lung cancer cell line was assessed by an MTT assay. The experiment was performed using different concentrations of the ethanolic extract of *T. roseo-alba* and its AgNPs ranging from 50, 100, 200, 300, 400 and 500µg. The effect of the samples on the cell viability is shown in Figure 40 and the cytotoxicity was documented as IC_{50} (µg/ml).

Figure 40. Cytotoxic effect of the ethanolic extract of *T. roseo-alba* and its AgNPs by MTT assay

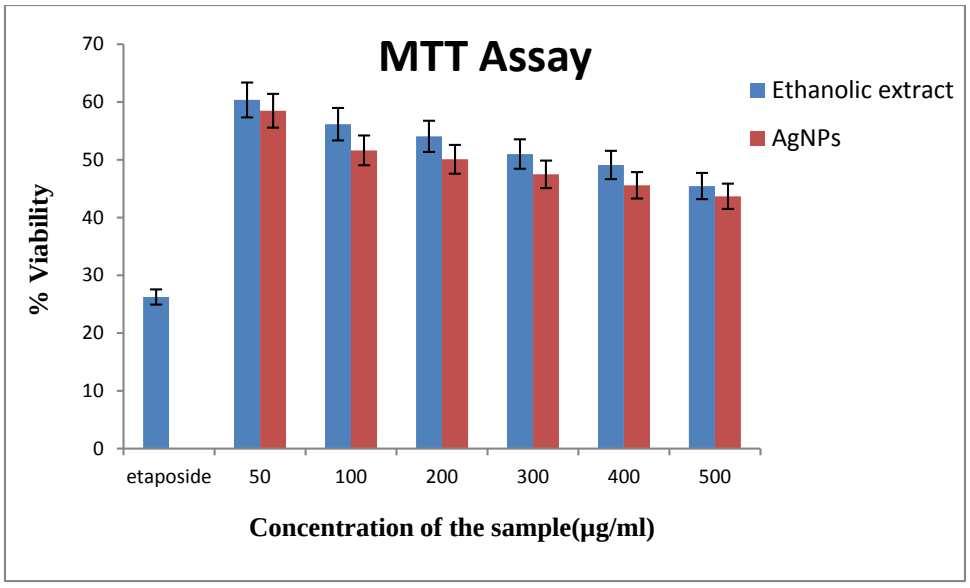

The findings of the present study revealed that the ethanolic extract of *T. roseo-alba* and its AgNPs were able to induce cell death in a concentration dependent manner. When A549 cell lines were treated with the samples, the viability of the cells were found

to be decreased even at the lowest concentration. Though both the samples were showing promising cytotoxic activity, AgNPs of *T. roseo-alba* was found to be more potent than the ethanolic extract. Further, greater cytotoxic effect was observed at their higher concentration (500µg). The IC_{50} value was found to be 300 µg/ml and 200 µg/ml for ethanolic extract of *T*. *roseo-alba* and its AgNPs respectively. The dimension of the NPs, the amount of Ag, and the coating agents contribute to greater cytotoxicity and decreased cell growth. Because of their increased cellular absorption and wide surface area for interaction with biomolecules, small NPs were found to be more cytotoxic (George *et al.,* 2018). The reduction in cell viability with increased concentration of the ethanolic extract of *T. roseo-alba* and its AgNPs revealed the ability of the plant to act as an effective drug for the treatment of cancer which could be attributed to the antioxidant and radical scavenging potential of the plant.

Similar to our Study, Robinson *et al*. (2017) evaluated anticancer potential of *Tecoma stans* on lung cancer cell line (A549) and reported efficient inhibition of cancer cell proliferation from 20µg/mL concentration. A study by Thomas *et al*. (2017) on anticancer activity of protein extracted from *Morinda pubescens* leaves against human cancer cell lines revealed the strong cytotoxic activity on A549 cells even at lowest concentration. The cytotoxic studies carried out by Esmaeilbeig *et al.* (2015) using 10 different medicinal plants on five tumor cells proved the antiproliferative ability of all the plant extract on Jurkat cell line and K562 cell line with greater than 50% inhibition.

Antitumor activity of *Orobanche crenata* methanolic extract was evaluated on diverse cancer cell lines by Hegazy *et al.* (2020). The findings from the study highlighted the abilities of *O.P crenata* extract in treatment of many cancers which may be ascribed to the existence of various secondary metabolites. In a study by Cyril *et al.* (2019), anticancer activity of silver nanoparticles synthesised using *Derris trifoliata* was proved on lung cancer cell line A549. Silver nanoparticles synthesized using *Camellia sinensis* were analysed for their antiproliferative potential on three different human cancer cell lines by Yadav *et al*. (2018) and they observed strong cytotoxicity against human leukemia cancer cell line MOLT-4 which may be owing to the presence of polyphenols and the protective activity is directly linked with the antioxidative potential of *Camellia sinensis*.

The cytotoxic effect of *T. roseo-alba* and its AgNPs might be ascribed to the presence of high content of bioactive metabolites like phenols and flavonoids, which may be responsible for the formation of green synthesized AgNPs. These principal bioactive

metabolites may have anti neoplastic potential and the ability to cause cell death by molecular processes such as activation of the autophagy, formation of ROS and apoptosis.

4.3.2 Determination of Apoptosis

4.3.2.1 Analysis of Apoptosis by Annexin V/FITC staining

Apoptosis performs a crucial role in the homeostasis and it is characterized by numerous morphological and biochemical alterations in cells (Ullah *et al.,* 2020). To determine apoptosis in lung cancer cells treated with IC_{50} concentrations of ethanolic extract *T. roseo-alba* and its AgNPs, FITC Annexin V and PI staining was performed which was followed by flow cytometer analysis. Under normal conditions, phosphatidylserine (PS) residues are present in the inner membrane of the cytoplasmic membrane of the cells. Phosphatidylinositol serine is translocated to the cell membrane during the early stages of apoptosis and can be stained with fluorescently labeled annexin V (Baharara *et al.,* 2015).

Figure 41. Flow cytometry analysis of A549 cells by double-labelling with Annexin V and PI dyes

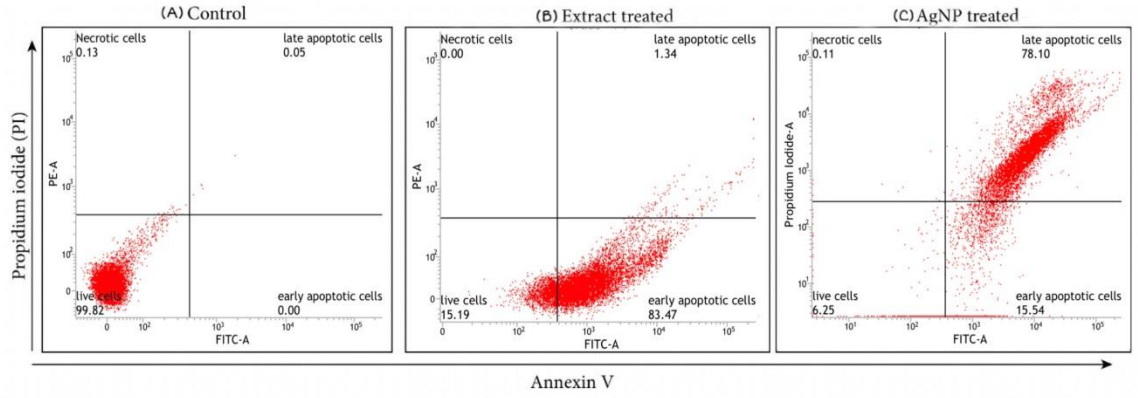

(A) Control (B) Ethanol extract of *T. roseo-alba* (C) AgNPs of *T. roseo-alba*

The outcomes of the present study demonstrated the induction of apoptosis in cancer cells exposed to ethanolic extract (300µg/mL) and AgNPs (200µg/mL) for 24 hours. The ethanolic extract and AgNPs induced cell death by Annexin V/FITC staining was studied by flow cytometry in Lung cancer cell line A549 is given in Figure 41.

The apoptotic and non-apoptotic cell population after the treatment with *T. roseo-alba* and its AgNps was evaluated by Annexin V/PI staining. Initiation of apoptosis was evident by the higher population of dead cells upon treatment. When the cells were treated with ethanolic extract of *T. roseo-alba*, they were seen in early apoptotic stage of cell death indicating the ability of the ethanolic extract to induce apoptosis and upon further treatment with its silver nanoparticles, the cells were observed in late apoptosis documenting the enhanced ability of AgNps to induce apoptosis and only very few cells are seen in early apoptosis. Since AgNPs of *Tabebuia roseo- alba* have directed the cells into late apoptosis it can be concluded that the synthesized AgNPs have the ability to induce apoptosis.

A study by George *et al.* (2018) demonstrated apoptotic efficacy of *Rubus*-conjugated AgNPs (RAgNPs) on human adenocarcinoma cells by Annexin V/PI staining. Results of the study evidenced the cell death in a concentration dependent way following the treatment of RAgNPs. Ullah *et al.* (2020) showed the ability of biosynthesized silver nanoparticles of *Fagonia indica* extract to induce apoptosis in MCF-7 breast cancer cells and they observed the changes in the population of viable cells due to the apoptotic potential of AgNps. The flow cytometry analysis using Annexin V-FITC/PI staining carried out by Xu *et al.* (2020) revealed that green synthesized silver nanoparticles of *Ginkgo Biloba* extract induced both early and late apoptosis via mitochondrial pathway in cervical cancer cells.

Apoptotic induction potential of silver nanoparticles synthesized using *Zataria multiflora* extract was studied by Baharara *et al*. (2018) in HeLa Cells. The results confirmed the apoptotic effect of *Zm*-AgNPs in a concentration-dependent manner. Another study by Al-kawmani *et al*. (2020) documented the apoptotic ability of *O. arabicus* synthesized AgNPs using Annexin V-FITC/PI staining and confirmed the anticancer potential of OA-synthesized AgNPs which is possibly due to the presence of flavonoid glycosides, that may be involved in the reduction process of silver nanoparticles.

Apoptosis has been established as a main cause of cell death when cells are exposed to green synthesized AgNPs (Farah *et al.,* 2016). The association of AgNPs with mammalian cells may cause oxidative stress by producing ROS at a concentration high enough to deplete cellular antioxidants that leads to genomic damage. Induction of oxidative stress and associated damage is one of the most significant mechanisms of

AgNP toxicity and it may promote apoptosis under various signals and pathological conditions (Suliman *et al.,* 2015). AgNPs enter cells through phagocytosis, pinocytosis, or endocytosis, interact with cellular material, and produce harmful oxygen radicals, which lead to DNA fragmentation and apoptosis (Dehghanizade *et al.,* 2017).

In agreement with above cited literature, the enhanced ability of AgNPs of *T. roseo-alba* to direct the cancer cells into late apoptotic phase may be attributed to the presence of high level of phenols and flavonoids, which may be responsible for the leaf mediated synthesis of silver nanoparticles. Therefore it can be inferred that *T. roseo-alba* and its AgNPs have been shown to cause oxidative stress, damage to cellular components, altered autophagy and eventually lead to cellular death and thus can be used as a novel lead molecule for the discovery of new anticancer drugs.

4.3.2.2 Analysis of Mitochondrial Membrane Potential by JC-1 staining

The cellular apoptotic mechanism is triggered when cells are destroyed by the development of reactive oxygen species in their internal environment during metabolic activity. Excessive ROS generation causes alterations in the mitochondrial membrane permeability, which harms the respiratory chain and causes cellular death. Mitochondria play an important role in cellular death, and alteration in the membrane permeability of the mitochondria is an initial incident in apoptosis. Numerous pro-apoptotic proteins are released into the cytoplasm by the mitochondrion, and a permeability transition pore is formed in the membrane of mitochondria.

Any alterations in the permeability of mitochondrial membrane can be detected by performing JC-1 staining. Because of the electrochemical potential gradient, the dye JC-1 accumulates in the mitochondrial matrix and forms J-aggregates, red fluorescent aggregates, in normal cells. JC-1 dye clustering in the mitochondria is prevented by deviations in the mitochondrial membrane potential and hence, it is distributed all over the cell. This results in a change in fluorescence from red (J-aggregates) to green (JC-1 monomers), indicating depolarization of the mitochondrial membrane (Ranjan *et al.,* 2020).

Thus, in the present study, the level of mitochondrial membrane potential was investigated using a flow cytometer after JC-1 staining. The proportion of cancer cells undergoing apoptosis was determined after treatment with ethanolic extract of *T. roseo-*

alba and its AgNPs at their respective IC_{50} concentrations. Results are demonstrated based on the red to green fluorescence ratio, where an increased ratio indicated viability of the cells and a lesser ratio indicated cell death. The control revealed higher red to green fluorescence ratio disclosing fully polarized mitochondria, which formed J-aggregates as red fluorescence. Treatment with ethanolic extract and their AgNPs, on the other hand, caused mitochondrial membrane depolarization in A549 cells, as evidenced by a decrease in red fluorescence and an increase in green fluorescence intensity indicating the ability of the *T. roseo-alba samples* to trigger apoptosis (Figure 42).

Figure 42. Flow cytometric analysis of A549 cell lines after staining with JC1

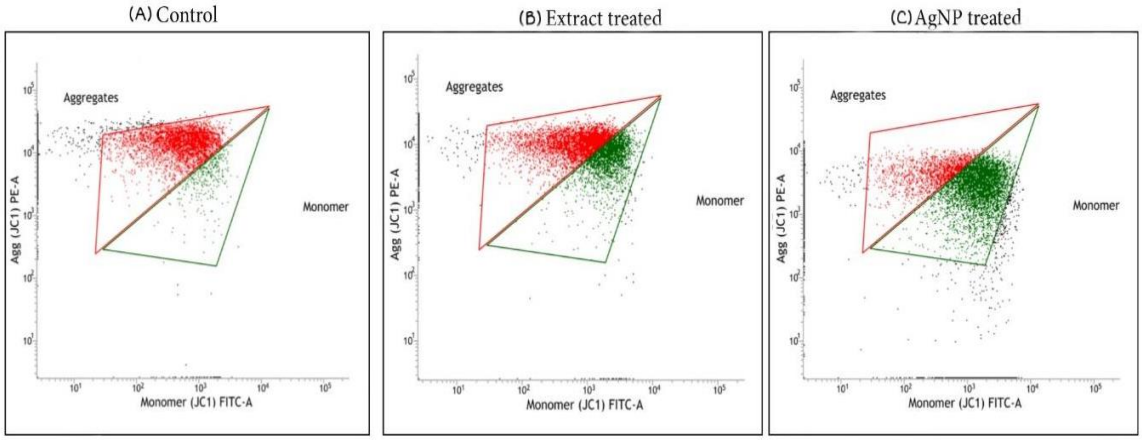

(A) Control (B) Ethanol extract of *T. roseo-alba* (C) AgNPs of *T. roseo-alba*

When compared to ethanolic extract, increased green fluorescence intensity was observed on exposure of AgNPs and this change in fluorescence pattern indicated the more pronounced ability of AgNPs to depolarize the mitochondrial membrane integrity leading to apoptosis induction and subsequent cell death. The depletion of membrane potential of mitochondria causes cytochrome C release into the cytoplasm and activates the upregulation of caspase-3 via caspase-9 pathway (Jabir *et al.,* 2021). These findings reiterate the ability of ethanolic extract of *T. roseo-alba* and its AgNPs to activate the intrinsic apoptotic signaling pathway which may be attributed to the generation of intracellular ROS and depletion of mitochondrial membrane integrity that ultimately results in the fragmentation of DNA and thereby causes cell cycle arrest signifying the antiproliferative activity of the ethanolic extract of *T. roseo-alba* and its AgNPs.

In line with our observations, Kanipandian *et al.* (2019) validated the triggering of the intrinsic apoptotic pathway by the interruption of mitochondrial membrane stability in the A549 lung cancer upon the treatment with silver nanoparticles of *Gossypium hirsutum* and subsequent changes in the expression of Apoptotic proteins. Yet another study by Jung *et al.* (2019) proved the anti-tumoral activity of the extracts of *Phyllodium elegans* on human cancer cell lines by the depolarization of mitochondrial membrane integrity and stimulation of cell death signalling by activating caspase-3/-9.

According to Gurunathan *et al.* (2015), treatment with *Bacillus tequilensis* and *Calocybe indica* silver nanoparticles resulted in a upsurge in mitochondrial depolarization, and reported a link between intracellular ROS production and induction of cellular death in human breast cancer cells through the intrinsic apoptosis pathway. In accordance with our study, Prasannaraj and Venkatachalam, (2017) demonstrated the loss in mitochondrial membrane integrity by green silver nanoparticles synthesized using four medicinal plants against cancer cell lines.

The results observed in our study are in agreement with the cited literature, treatment with ethanolic extract and their AgNPs of *T. roseo-alba*, caused depolarization of the mitochondrial membrane potential, cytochrome C release thereby triggering cells to undergo apoptosis through intrinsic pathway. The results of the cell line analysis performed using the candidate plant chosen for the present study clearly depicts the presence of active principles in the extract which could mediate scavenging action of the radicals generated and also coordinate nanoparticle formation. This in turn could readily affect the membrane stability of the mitochondria and initiate programmed cell death and interrupt cell cycle events proving its anti proliferative action in cancer cells which could aid lead molecules for drug designing against oxidative stress induced diseases like cancer.

4.3.2.3 Analysis of DNA Fragmentation

To obtain more perceptions into the method of cell death caused by ethanolic extract of *T. roseo-alba* and its AgNPs, its effect on the DNA fragmentation was determined. Induction of apoptosis in A549 cells was validated by DNA fragmentation analysis using gel electrophoresis technique, as evidenced by a dose-dependent rise in DNA fragmentation upon treatment. The banding pattern observed (Figure 43) indicates the occurrence of DNA shearing and fragmentation in the lanes treated with the increasing concentration of *T. rosea alba* and its AgNPs indicative of apoptosis induction.

The outcomes of the present study are in par with the results of Badgujar *et al.* (2018) who observed DNA fragmentation in A549 cells treated with *B. monosperma* chloroform extract. Similar results were also observed by Rajavel, *et al.* (2017) using benzene extract *Grewia tiliaefolia* on A549 cells and based on the results apoptotic mediated cell death was confirmed.

Figure 43. DNA fragmentation by *T.roseo-alba* and its AgNPs

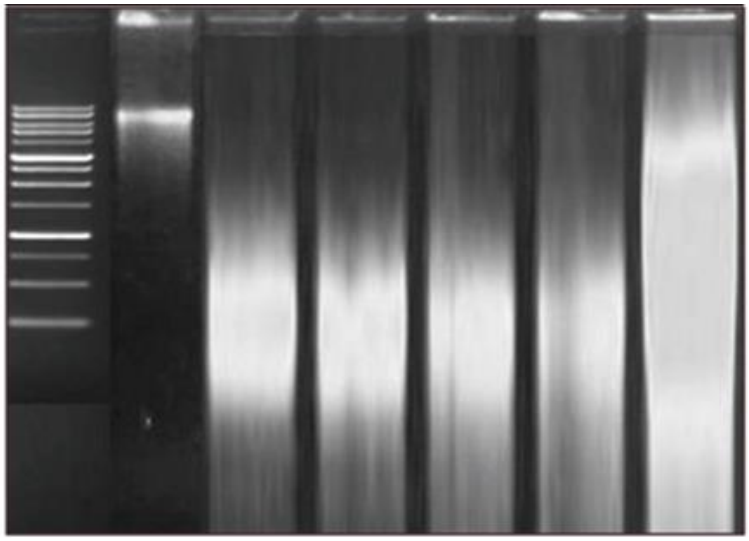

M C 1 2 3 4 5

M. ladder marker

1 200µg/ml treated with ethanolic extract of *T. roseo-alba*

2 400µg/ml treated with ethanolic extract of *T. roseo-alba*

3 500µg/ml treated with ethanolic extract of *T. roseo-alba*

4 400µg/ml treated with AgNPs of *T. roseo-alba*

5 500µg/ml treated with AgNPs of *T. roseo-alba*

4.3.2.4 Western blotting Analysis

As described in our present study, ROS are generated by an ethanolic extract of *T. roseo-alba* and its AgNPs, which causes inhibition of cell-cycle at specific checkpoints in A549 cells which results in self-mediated cellular death or DNA repair process. Variations in certain protein expressions cause cellular apoptosis via mitochondrial pathway. Caspases are recognised to perform a key part in apoptosis execution and initiation, and they are stimulated in many cells throughout this process. The role of activated caspase-3 in genomic fragmentation and programmed cell death is crucial. Caspases 3 has been shown to cleave and translocate caspase-activated DNAse (CAD) upon activation, resulting in DNA fragmentation (Ullah *et al.,* 2020).

Variations in the Bax/Bcl ratio cause outer mitochondrial membrane permeabilization, release soluble proteins from the inter membrane gap into the cytosol, enhance activation of caspase. Effector caspase (Caspase-3) is activated by activates caspase-9, the activated caspase 3 cleaves substrates at aspartate residues, and this appears to be a prominent apoptotic incident (Ranjan *et al.,* 2020).

Thus, to investigate the effect of ethanolic extract of *T. roseo-alba* and its AgNPs on the apoptotic pathway, the caspase-3 enzyme activity was examined in A549 cells through western blotting. As predicted, upon treatment with ethanolic extract of *T. roseo-alba* and its AgNPs, the level of caspase 3 expression was observed to be concentration dependent. The treatment with ethanolic extract of *T. roseo-alba*, triggered apoptosis in A549 cells displaying an up-regulation of the active forms of caspases 3. Further, when A549 cells treated with AgNPs of *Tabebuia roseo- alba*, more pronounced expression levels of caspases-3 were observed compared to ethanolic extract of *T. roseo-alba* as shown in Figure 44 and 45.

Figure 44. Western blotting analysis for caspase 3 expression on human lung cancer A549 cells treated with ethanolic extract of *T. roseo-alba*

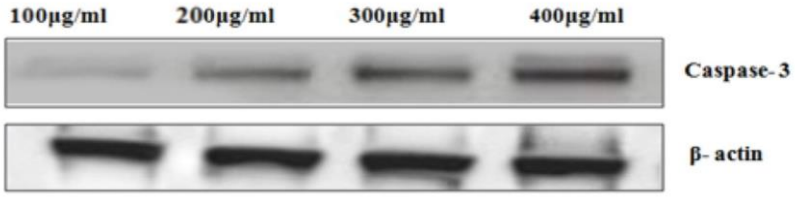

(a) Protein abundance of active caspase 3 and control β-actin

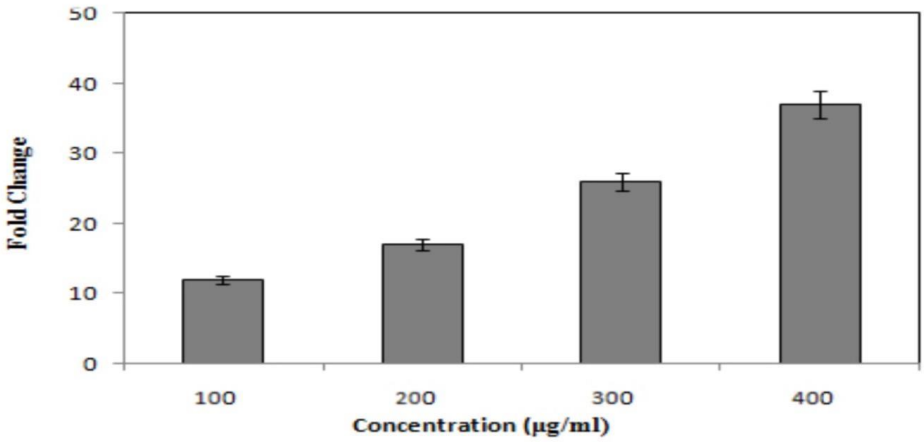

(b) Densitometry for the protein abundance of active caspase 3.

Figure 45. Western blotting analysis for caspase 3 expression on human lung cancer A549 cells treated with silver nanoparticles of *T. roseo-alba*

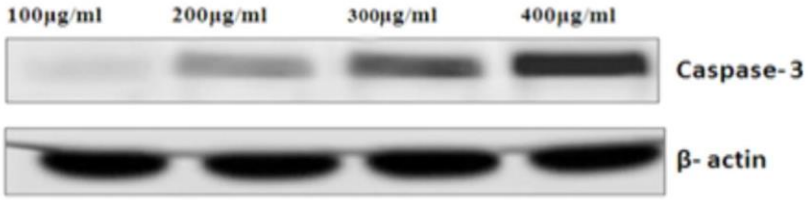

(a) Protein abundance of active caspase 3 and control β-actin

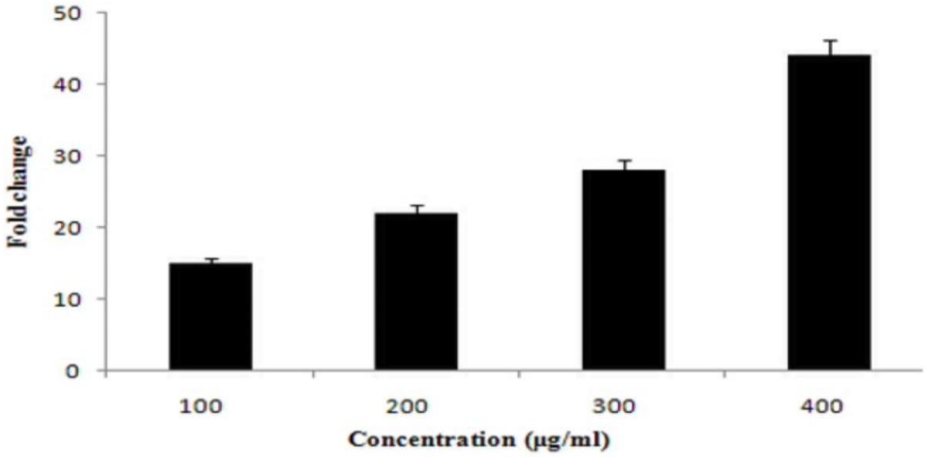

(b) Densitometry for the protein abundance of active caspase 3.

Similar results were observed by Meenakshisundaram *et al.* (2020), in which the expression levels of cleaved caspase-9, caspase-8 and caspase-3 were increased in A549 cells treated with AgNPs synthesised from *Annona muricata*. In line with our study, the increased caspase 3 activity in a concentration dependent manner was observed in AgNP-treated osteosarcoma cells, by Fageria *et al.* (2017) using mycogenic protein-capped AgNPs. Western blot analysis by Pannerselvam *et al.* (2020) reported higher expression levels of caspases-3 and 9 in human breast cancer cells treated with synthesized asian spider flower silver nanoparticles. An increase in the active caspase-3 level was also observed in MCF-7 cells treated with AgNPs of *Magnolia champaca* by Antony *et al.* (2021).

Thus, treatment with ethanolic extract of *T. roseo-alba* and its AgNPs mediated apoptosis by intrinsic pathway. The change in membrane potential causes the development of a transition pore in mitochondria, which leads to the release of cytochrome C, which initiates the caspase cascade resulting in DNA fragmentation.

4.3.3 Analysis of Cell cycle

Apoptosis and cell cycle arrest are inextricably linked because apoptosis occurs when cell proliferation is disrupted at specific cell cycle checkpoints. When DNA damage occurs in cells, a checkpoint in each step of the cell cycle is responsible for halting cell growth until the damage is repaired, or if the damage cannot be repaired, cells undergo apoptosis (Yakop *et al.,* 2018). The effect of ethanolic extract of *T. roseo-alba* and its AgNPs on the cell cycle distribution of A549 cells were examined using a flow cytometer. As depicted in Figure 46, the cells treated with ethanolic extract at their IC_{50} concentration were arrested at the G2/M transition stage which was evidenced by the increased percentage of the cell population. Thus, the rise in the apoptotic cell population observed in this phase proved the ability of ethanolic extract treated A549 cells to pass through G2 checkpoint and therefore, G2/M transition was shown to be disrupted upon treatment with ethanolic extract.

Further treatment with silver nanoparticles blocked the cell cycle at G0-G1 checkpoint and the cells were found to be quiescent. In contrast, the untreated control cells were distributed in all the phases of the cell cycle and the results further supported the more pronounced apoptotic inducing ability of AgNPs of *T. roseo-alba* compared to ethanolic extract.

Figure 46. Flow cytometric analysis of cell cycle distribution of A549 cells.

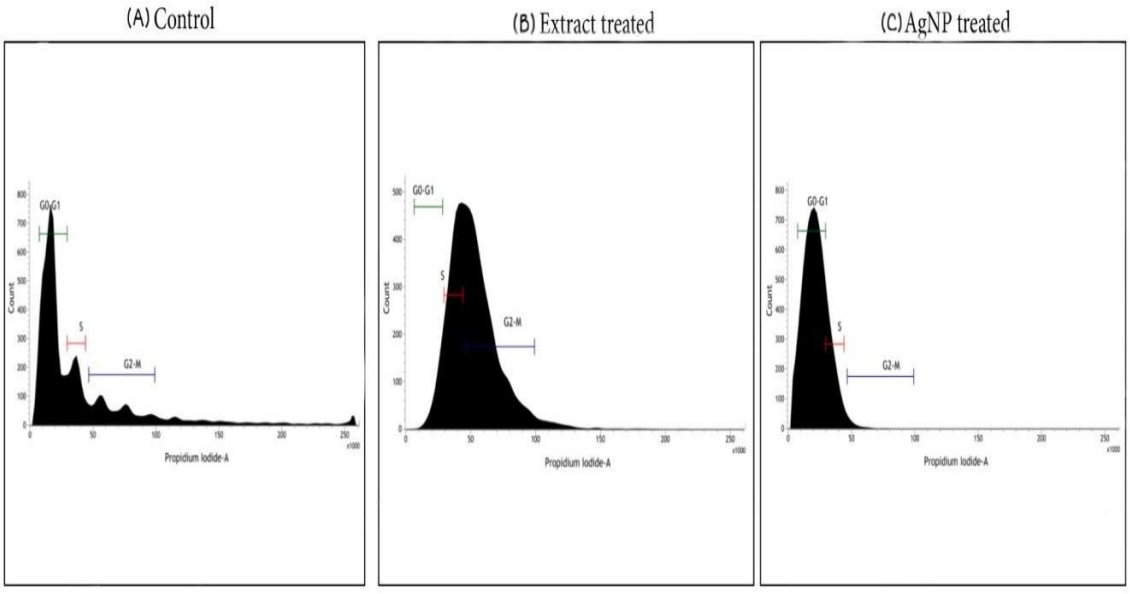

(A) Control (B) Ethanol extract of *T. roseo- alba* (C) AgNPs of *T. roseo- alba*

The present study is in concordance with the work done by Kuppusamy *et al.* (2016) which stated AgNPs caused colon cancer cells (HCT-116) growth arrest at Sub-G1 phase. A Study done by Al-Sheddi *et al.* (2018) reported the growth inhibition of Human Cervical Cancer Cells HeLA by *Nepeta deflersiana*-AgNPs and G2/M transition was shown to be affected. In par with our study, cell cycle arrest in the sub G1 phase was documented upon treatment with *M. modestum* methanolic leaf extract in a study carried out by Pumiputavon *et al*. (2017). Yet another study by Yakop *et al.* (2018) reported the induction of apoptosis through G1 cell cycle arrest in oral squamous cell carcinoma cell lines upon the treatment with silver nanoparticles of *Clinacanthus nutans* leaves.

Cell cycle analysis done using the samples of *T. roseo-alba* revealed that the cancer cell lines A549 were able to undergo cell cycle arrest proving their antiproliferative effect. Cells treated with *T. roseo-alba* caused cell cycle phase transition and arrest cells at G2/M phase whereas the green synthesised nanoparticles could arrest at G0/G1 phase indicating the prominent effect of nanoparticles when compared to the crude extract. Thus the results obtained from the flow cytometer analysis proved the ability of AgNPs in the control of cancer cell proliferation by blocking the cell cycle at specific checkpoints that suppress the progression of cancer.

The results revealed that both the ethanolic extract of *T. roseo-alba* and its AgNPs were proved to enforce toxicity to the lung cancer cells in a concentration dependent manner. The apoptosis-inducing ability and antiproliferative potentials of *T. roseo-alba* leaves were ascribed to the major bio-active molecules like polyphenols and flavonoids present in them. The ethanolic extract of *T. roseo-alba* and its AgNPs also increased the level of intracellular ROS and amplified autophagy and apoptosis rate by inducing membrane permeability, causing depolarization of mitochondrial membrane potential which was evident from Annexin V/FITC and JC-1 staining. Treatments with the ethanolic extract of *T. roseo-alba* and its AgNPs caused upregulation of caspases 3 which triggered the apoptotic pathway and caused cell demise. Furthermore, cell cycle analysis using the ethanolic extract of *T. roseo-alba* and its AgNPs brought build-up of cells in the G2/M and G0-G1 phase, respectively, displaying apoptotic cell death population. Based on the results obtained it may be concluded that, silver nanoparticles of *T. roseo-alba* leaf extract showed more pronounced apoptotic induction and antiproliferative activity than the ethanolic extract of *T. roseo-alba* and thus it can be considered as a capable anticancer drug in lung cancer therapeutics.

Phase IV

To ascertain the drug efficiency of the extract, *insilico* studies were done to confirm the interactions of the bioactive compounds of the *T. roseo-alba* extract and the proteins involved in apoptotic and cell signaling pathways associated with lung cancer. The ligands were docked to the target proteins using Autodock Tools 4.2.6. The results obtained after the interaction of ligands and proteins were assessed based on the important parameters namely binding energy, H-bonds and good contacts, which give information about the binding affinity of ligands towards the receptor.

4.1 i*n silico* docking of bioactive compounds of the *T. roseo-alba* with apoptotic regulators and lung cancer targets

One of the most prominent processes in the pharmaceutical industry is drug development. With the rapid development of computer technology, screening lead molecules for drug designing and discovery have advanced considerably using computer assisted technologies that greatly reduce the period and expense of drug development. In general, identification of potential target proteins for drug screening and designing is made possible with bioinformatics which contribute in disclosing the vital genes from a huge genomic data bank (Lin *et al.,* 2020). The use of computational platforms help to reveal biological effects, target specificity and effects at molecular level and also the pharmacodynamic, pharmacokinetic and toxicological characterization of natural compounds (Thomford *et al.,* 2018)**.**

Hence the present study was carried out to dock phytoconstituents of *T. roseo-alba* against molecular targets of apoptotic and cell signaling pathways associated with lung cancer**.** Around 11 phytoconstituents identified from the *T. roseo-alba* by the chromatographic techniques were chosen and prepared for docking studies.

4.1.1. ADMET ANALYSIS

The Absorption, Distribution, Metabolism, Excretion and Toxicology (ADMET) properties of those drugs were studied using Swiss ADME tool. The results are tabulated in the following Table 6.

Table 6. Analysis of ADME properties of the retrieved compounds from *T. roseo-alba*

Molecule and Molecular formula	Molecular Weight (g/mol)	No. of Rotatable bonds	No. of H-bond acceptors	No.of H-bond donors	Molar Refractivity (MR)	Partition Coefficient (iLOGP)	Gastro Intestinal absorption	Blood-Brain Barrier permeant	Lipinski's violations
Squalene (C30H50)	410.72	15	0	0	143.48	6.37	Low	No	1
2-Hexadecen-1-ol (C16H32O)	240.42	13	1	1	79.71	4.25	High	Yes	1
Neophytadiene (C20H38)	278.52	13	0	0	97.31	5.05	Low	No	1
9-Eicosyne (C20H38)	278.52	14	0	0	96.42	5.43	Low	No	1
Stigmast-5-en-3-ol (C29H50O)	414.71	6	1	1	133.23	4.79	Low	No	1
2-Hexadecene (C16H32)	224.43	12	0	0	78.55	4.67	Low	No	1
Rutin(C27H30O16)	610.52	**6**	16	10	141.38	2.43	Low	No	3
Colchicine (C22H25NO6)	**399.44**	**6**	**6**	**1**	**109.36**	**3.13**	**High**	**No**	**0**
Nicotinic Acid (C6H5NO2)	**123.11**	**1**	**3**	**1**	**31.2**	**0.86**	**High**	**No**	**0**
Gallic Acid (C7H6O5)	**170.12**	**1**	**5**	**4**	**39.47**	**0.21**	**High**	**No**	**0**
Quercetin (C15H10O7)	**302.24**	**1**	**7**	**5**	**78.03**	**1.63**	**High**	**No**	**0**

Among 11 retrieved compounds, only 4 compounds- Gallic acid, Nicotinic acid, Colchicine and Quercetin showed the drug-likeness as they have'0' violations with Lipinski's RO5 and these ligands can be used for further studies to develop a potential drug.

4.1.2. Molecular Docking Analysis

Molecular docking is a well-recognized structure-based *in silico* approach that is generally employed in computer assisted-drug design (CADD). This technique allows the discovery of new drugs, the prediction of ligand-target connections at the molecular level (Pinzi *et al.,* 2019).

4.1.2.1 Docking Analysis with Bcl2 family members

The anti-apoptotic and pro apoptotic members of the Bcl-2 family are the well-studied molecules in programmed cell death. Anti-apoptotic proteins like Bcl-2 and Bcl-xL inhibit apoptosis, whereas pro-apoptotic proteins like Bax and Bak cause death

antagonists to release caspases, causing apoptosis. Therefore, the Bcl-2 family of proteins perform a vital role in the regulation of apoptosis and its overexpression has been related to a variety of cancers (Salam *et al.,* 2019).

Table 7. Docking interactions with members of the Bcl-2 family

Target Type	Target & PDB ID	Ligand &PubChem ID	BE (kCal/mol)	kI (μM)	No.of Bonds	Interacting Residues	Bond Length (Å)
Apoptotic Regulator	**Bcl2 (1g5m)**	Gallic Acid (370)	-3.60	0.223	3	TYR9	2.1 (H-O)
						ASN182	2.1 (O-H)
						TRP195	1.7 (H-O)
		Nicotinic Acid (938)	-3.62	0.002	3	TYR9	1.8 (H-O)
						ASN182	2.2 (O-H)
						TRP195	2.0 (H-H)
		Colchicine (6167)	-6.04	37.18	2	ASP10	2.2 (O-H)
						THR47	1.9 (H-O)
		Quercetin (5280343)	-3.15	2.00	3	ARG12	2.7 (H-O)
						ASP31	2.5 (O-H)
						ASP35	3.5 (O-O)
	Bcl-XL (3ZK6)	Gallic Acid (370)	-3.51	2660	2	ILE81	1.8 (O-H)
							2.7 (N-O)
		Nicotinic Acid (938)	-3.5	2700	2	ILE81	1.9 (O-H)
							2.8 (N-O)
		Colchicine (6167)	-4.31	696	3	SER4	3.6 (O-O)
						TRP188	2.8 (N-O)
						ASP189	3.1 (N-O)
		Quercetin (5280343)	-4.15	2900	2	GLU129	2.8 (O-H)
						ALA142	3.4 (O-O)

Among the compounds used for docking, Colchicine docked with Bcl 2 and exhibited best binding energy of -6.04 kCal/mol with the inhibition constant (kI) 37.18μM and the ligand efficiency of -0.40 kCal/mol (Table 7 and Plate 6). Two bonds were formed with the residues, ASP10 and THR47 of lengths 2.2Å and 1.9Å respectively.

Plate 6. Docking interactions of reported phytoconstituents of *T. roseo- alba* with members of the Bcl-2 family – Bcl-2

Bcl2 vs Gallic Acid

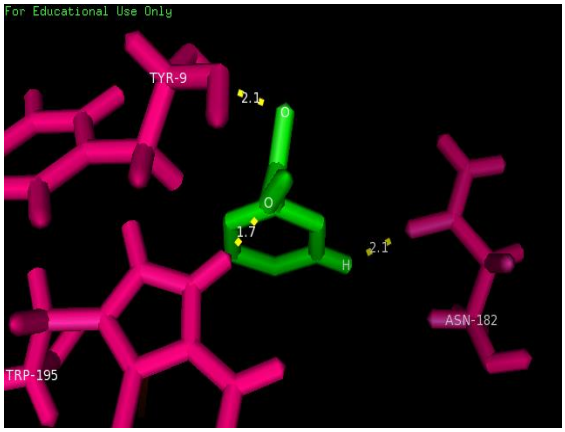

Bcl2 vs Nicotinic Acid

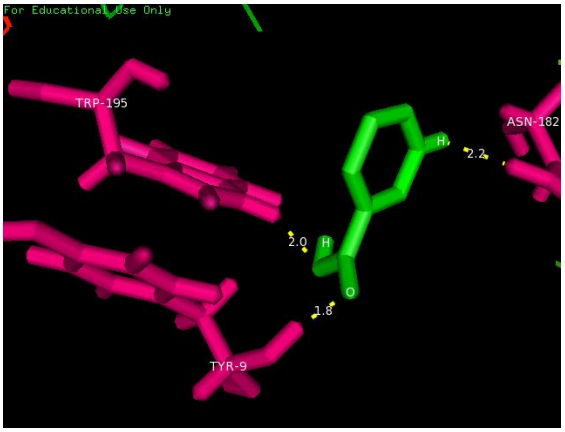

Bcl2 vs Colchicine

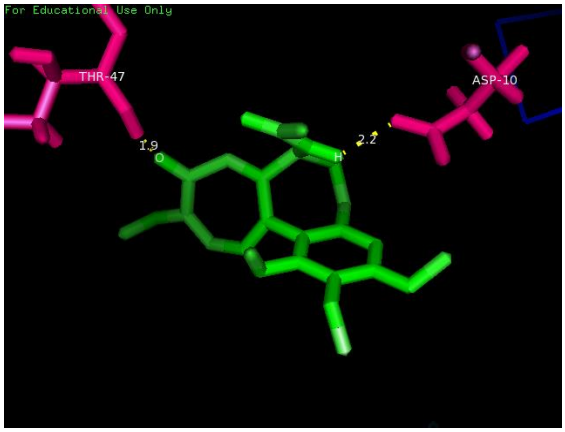

Bcl2 vs Quercetin

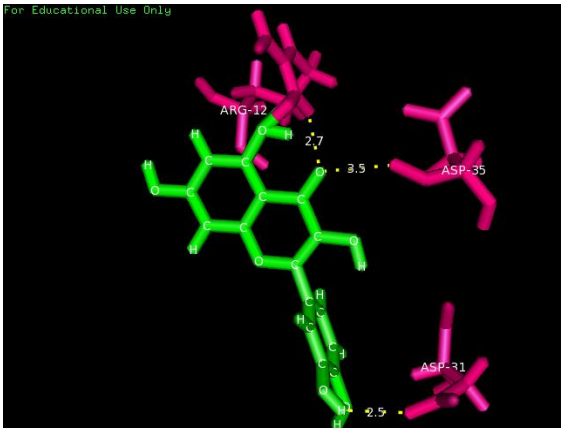

On performing the docking studies with the chemical constituents of *T. roseo-alba* against Apoptotic target Bcl XL, it was found that colchicine had the highest affinity with the binding energy of -4.31kCal/mol (Table 7 and Plate 7).

Plate 7. Docking interactions of reported phytoconstituents of *T. roseo-alba* with members of the Bcl-2 family-Bcl XL

Bcl XL vs Gallic Acid

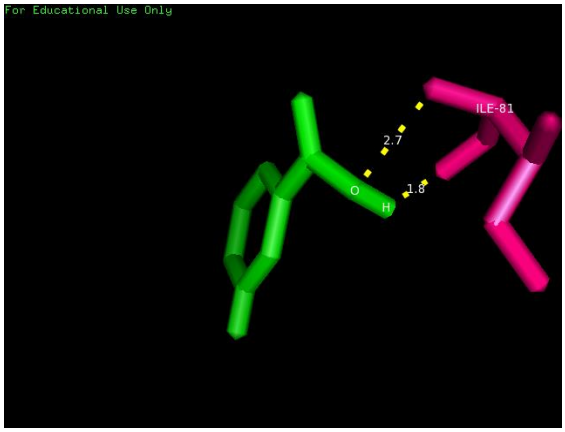

Bcl XL vs Nicotinic acid

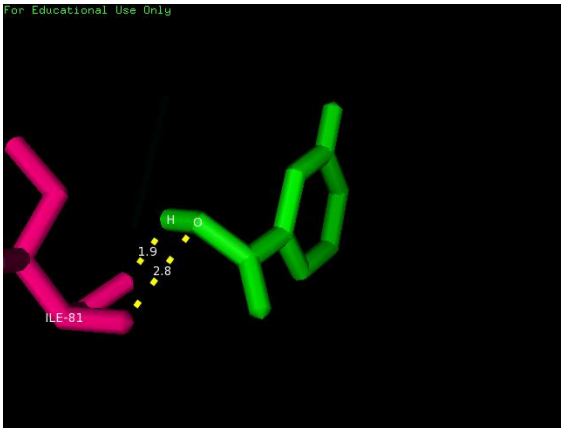

Bcl XL vs Colchicine

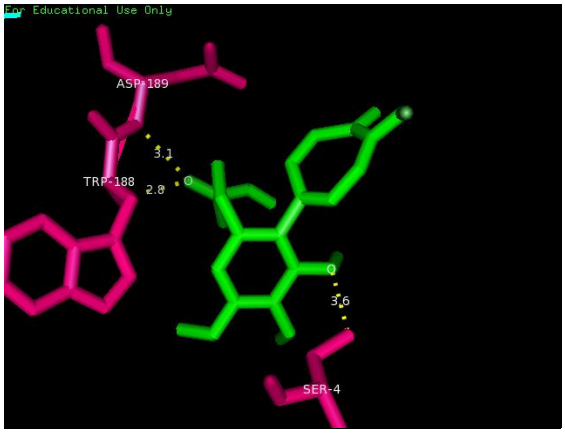

Bcl Xl Quercetin

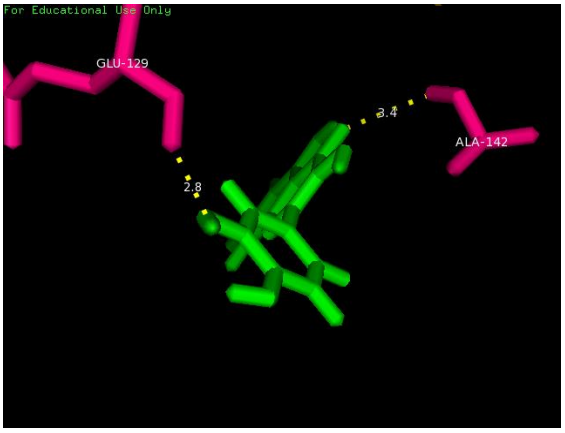

Thus the docking scores of Bcl 2 family members revealed that the selected compounds from *T. roseo-alba* readily interacted with the targets obtained from apoptotic pathways. This created strong evidence that the ligands considerably block the activity of target protein and suggest the possible inhibition leading to apoptotic cell death. Therefore, the phytoconstituents of *T. roseo-alba* can be used to modulate the pathways involved in cell death, thereby providing a suitable drug candidate.

4.1.2.2 Molecular Docking Analysis with proto-oncogene P53

Antioncogenes, also known as tumour suppressor genes, are a set of genes that regulate cell growth by limiting cell propagation and maintaining genome stability. *KRAS* and TP53 mutations were the initial documented mutations in NSCLC. *KRAS* mutations

are most commonly seen in colon, pancreatic, and lung carcinomas, whereas somatic TP53 mutations are found in nearly all form of cancer, with the maximum prevalence in ovarian, oesophageal, colorectal, head and neck, larynx, and lung malignancies (Wadowska *et al.,* 2020).

The most recurrently mutated gene in human malignancies is TP53 gene, with missense mutations accounting for the majority of TP53 alterations. Therefore, mutant p53 (mutp53) either loses the tumour suppressor function of wild type p53 (wtp53) or has a dominant negative influence on wtp53. Furthermore, certain mutants of the mutp53 gene have developed new carcinogenic functions (gain of function). These mutp53 proteins build up in cells and encourage progression of cancer. As a result, targeting mutp53 for degradation could be a valuable cancer preventive strategy (Tong *et al.,* 2020).

Table 8. Docking interactions with Mutant p53

Target Type	Target & PDB ID	Ligand &PubChem ID	BE (kCal/mol)	kI (μM)	No.of Bonds	Interacting Residues	Bond Length (Å)
Proto-Oncogene	**mutant p53 (4mzi)**	Gallic Acid (370)	-8.65	0.4568	4	ALA159	2.2 (O-H)
						VAL173	2.1 (2.1)
						LEU194	3.0 (N-O)
						HIS214	2.6 (N-H)
		Nicotinic Acid (938)	-5.56	83.9	4	SER96	2.9 (N-O)
						THR211	2.2 (O-H)
						ARG213	2.9 (N-O)
							3.2 (N-O)
		Colchicine (6167)	-6.0	40.29	2	ARG110	3.1 (N-O)
						TYR126	2.6 (O-O)
		Quercetin (5280343)	-5.1	182.37	8	GLN100	2.0 (O-H)
							2.9 (O-O)
						THR102	2.5 (O-O)
							2.8 (N-O)
						SER209	2.6 (O-O)
							3.4 (O-O)
						GLU271	1.8 (O-H)
							2.0 (O-H)

Though all the compounds were able to dock the selected target proto-oncogene Mutant p53, Gallic acid was found to have more binding efficiency when compared with other compounds, (Table 8 and Plate 8) which is evident from the binding energy (-8.65 kCal/mol) and ligand efficiency (-0.96 kCal/mol). The inhibition constant (kI) was found to be 0.4568µM. The compound forms 4 bonds with the residues ALA159, VAL173, LEU194 and HIS214 of lengths 2.2Å, 2.1Å, 3.0Å and 2.6Å respectively.

Plate 8. Docking interactions of reported phytoconstituents of *T. roseo-alba* with proto-oncogene mutant p53

mutant p53 vs Gallic Acid

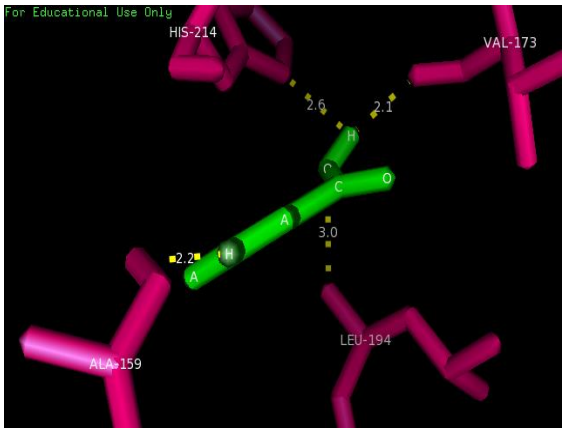

mutant p53 vs Nicotinic Acid

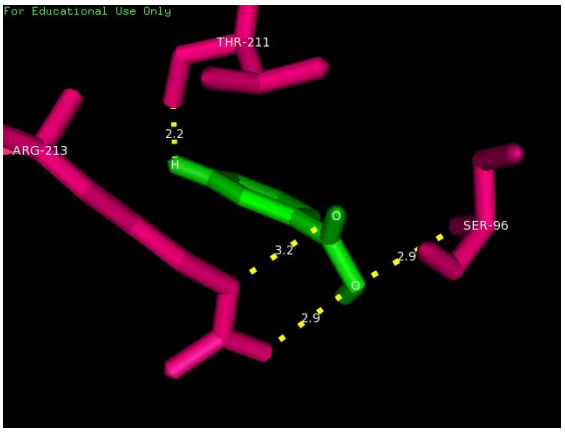

mutant p53 vs Colchicine

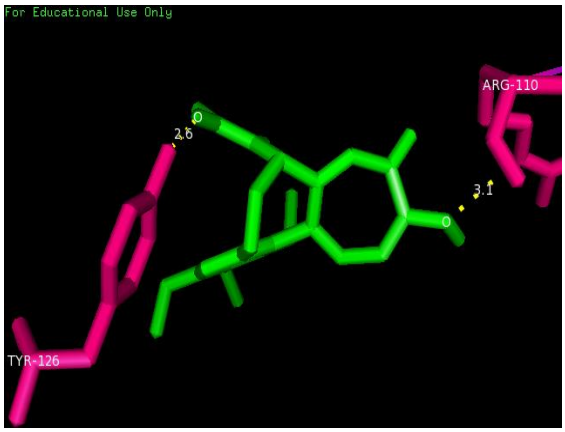

mutant p53 vs Quercetin

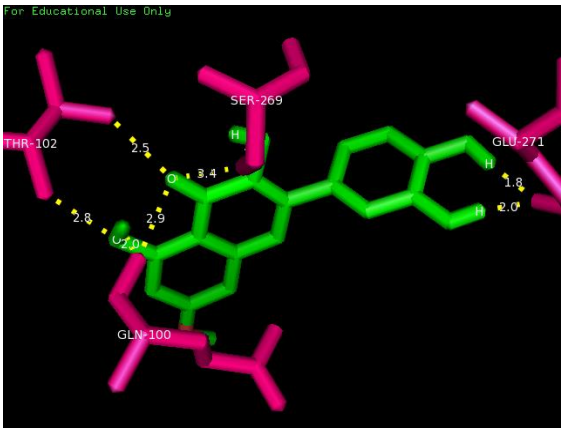

From the results, it is suggested that the identified compounds from *T. roseo-alba* can be used as appropriate drug leads against mutated p53 protein, to restore the functional mutant p53, leading to suppression of cancer progression.

4.1.2.3 Molecular Docking Analysis between Lung cancer targets

Mutations in the *KRAS* and EGFR genes are almost exclusively found in lung adenocarcinomas (Wadowska *et al.,* 2020)**.** In non–small cell lung cancer, the *KRAS* gene mutation is linked to a poor prognosis and drug resistance. The ability of *KRAS* to hydrolyze GTP is impaired by mutations and thus cause constitutive activation of its effector pathways which results in growth and progression of cancer (Ghimessy *et al.,* 2020).

Table 9. Docking interactions with mutant *KRAS* and EGFR

Target Type	Target & PDB ID	Ligand &PubChem ID	BE (kCal/mol)	kI (μM)	No.of Bonds	Interacting Residues	Bond Length (Å)
Lung Cancer	**mutant K-ras (4luc)**	Gallic Acid (370)	-6.1	33.98	7	GLY13	1.9 (H-O)
						VAL14	2.8 (H-O)
						GLY15	2.2 (H-O)
						LYS16	2.2 (H-O)
							2.2 (H-O)
							2.4 (H-O)
						TYR32	2.1 (O-H)
		Nicotinic Acid (938)	-6.0	40.04	8	GLY13	1.9 (H-O)
						VAL14	2.6 (H-H)
						GLY15	2.2 (H-O)
							2.3 (H-O)
						LYS16	2.1 (H-O)
							2.3 (H-O)
							2.4 (H-O)
						TYR32	2.3 (O-H)
		Colchicine (6167)	-5.93	44.9	4	ASN116	1.9 (H-O)
						LYS117	1.8 (H-O)
						ALA146	2.7 (H-O)
						LYS147	2.2 (H-O)

Target Type	Target & PDB ID	Ligand &PubChem ID	BE (kCal/mol)	kI (μM)	No.of Bonds	Interacting Residues	Bond Length (Å)
		Quercetin (5280343)	-6.75	11.3	7	GLY13	2.5 (H-O)
						LYS16	2.6 (H-O)
						SER17	2.2 (O-H)
						VAL29	2.0 (O-H)
						TYR32	2.2 (H-O)
						ASN116	1.9 (H-O)
						ALA146	2.6 (H-O)
Lung cancer	**mutant EGFR (3IKA)**	Gallic Acid (370)	-3.73	1830	4	GLY696	2.9 (N-O)
						LEU862	2.2 (O-H)
						ARG831	3.1(N-O)
							3.0 (N-O)
		Nicotinic Acid (938)	-3.96	1250	3	LYS728	2.6 (N-O)
						GLU1004	2.2 (O-H)
							2.8 (N-O)
		Colchicine (6167)	-3.91	1370	2	LYS875	3.5 (N-O)
							3.1 (N-O)
		Quercetin (5280343)	-4.4	2590	4	LYS745	2.8 (N-O)
						GLU749	1.6 (O-O)
						LEU858	2.7 (O-H)

Visualization of these interactions showed that, the compound quercetin was effective in docking against the target mutant *K-ras* resulting in the formation of 7 bonds with the residues GLY13, LYS16, SER17, VAL29, TYR32, ASN116 and ALA146 of lengths 2.5Å, 2.6 Å, 2.2 Å, 2.0 Å, 2.2 Å, 1.9 Å and 2.6Å respectively (Table 9 and Plate 9). The binding energy, ligand efficiency and the inhibition constant (kI) were -6.75kCal/mol, -0.31kCal/mol and 11.3μM respectively.

Plate 9. Docking interactions of reported phytoconstituents of *T. roseo-alba* with mutant *KRAS*

mutant *KRAS* vs Gallic Acid

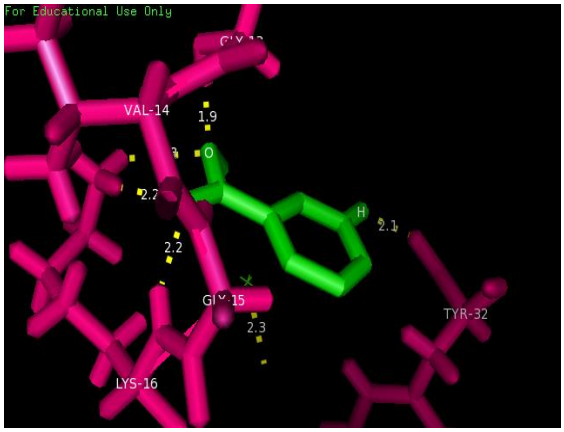

mutant *KRAS* vsNicotinic Acid

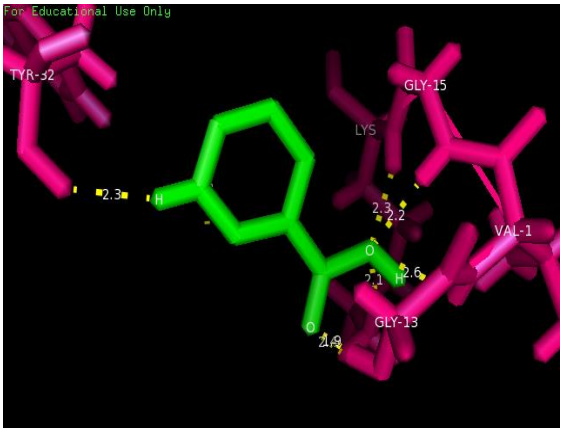

mutant *KRAS* vs Colchicine

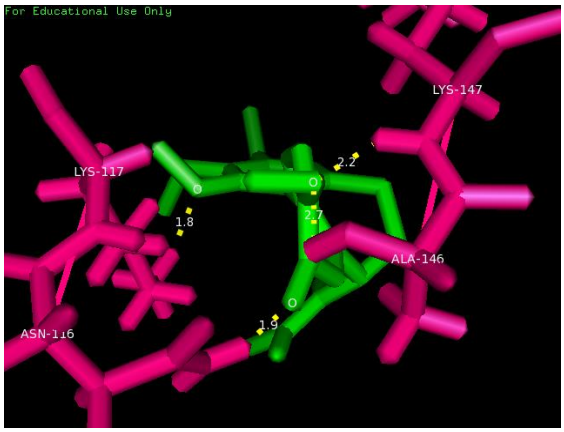

mutant *KRAS* vs Quercetin

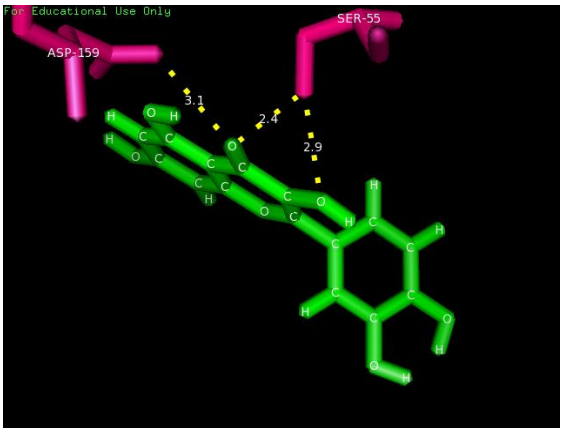

EGFR, a member of the ErbB family of receptor tyrosine kinases, regulates major functions associated with growth and differentiation of the cell through cellular signalling pathways. Because the EGFR protein is often overexpressed in many human malignancies including non-small cell lung cancer, targeting this molecule is considered as the promising approach in cancer therapeutics (Aiebchun *et al.,* 2021).

Plate 10. Docking interactions of reported phytoconstituents of *T. roseo-alba* with Mutant *EGFR*

Mutant EGFR vs Gallic Acid

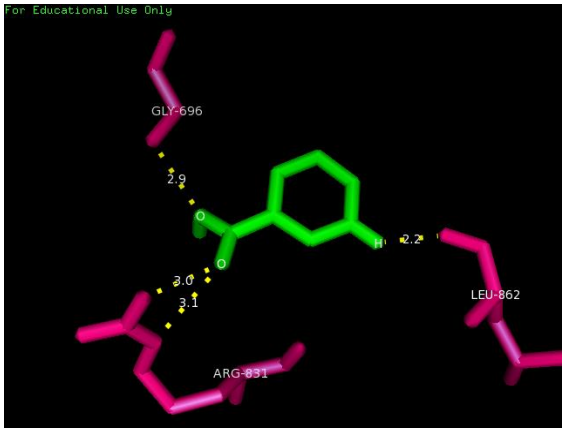

Mutant EGFR vs Nicotinic acid

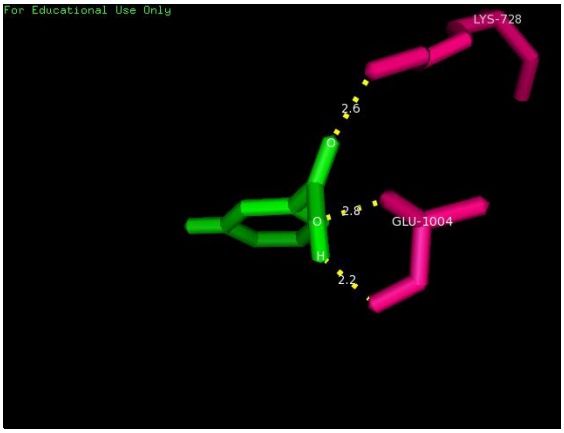

Mutant EGFR vs Colchicine

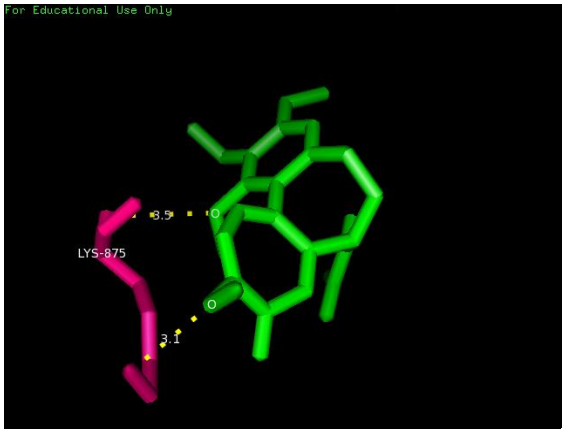

Mutant EGFR vs Quercetin

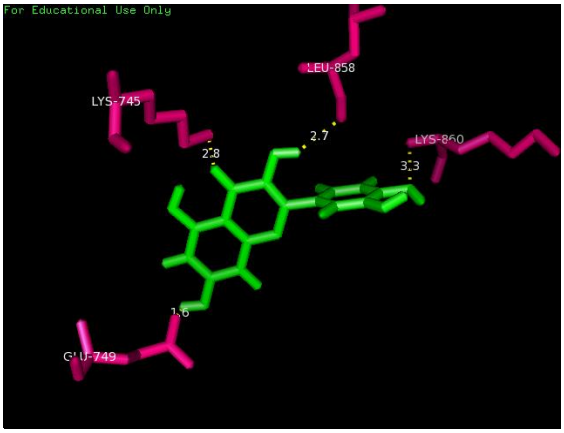

Analysis of docking results suggests that quercetin docked well into EGFR and the docking score was -4.4 kcal/mol. Three residues, LYS745, GLU749 and LEU858, residing in the binding site of EGFR ligand had hydrophobic interactions with quercetin (Table 9 and Plate 10).

Further based on the negative and lowest energy values of the interactions, the strong interaction between the lung cancer targets, (Mutant *KRAS* (4luc) and mutant EGFR) and other ligands, it can be concluded that several allosteric sites on the *KRAS* mutant and EGFR could be targeted by constituents of *T. roseo-alba*. Inhibition of these proteins by the active compounds of *T. roseo-alba*, might influence the signaling pathway associated with regulation of cell growth and thus can be used as the suitable

chemo preventive anti-cancer drug against lung cancer. The abnormal activation of the signaling cascades leads to uncontrolled proliferation of cells and inhibition of apoptosis induces the oncogene pathway for increasing the severity of disease condition (Durga and Julius, 2020).

In silico analysis on capsaicin and apoptotic targets revealed the higher affinity between the ligand and the selected targets with high binding energies thus proving its ability in the induction of apoptosis (Roy *et al.,* 2020). In a study by Radha and Padma, (2019) binding interactions between the compounds present in the leaves *Majorana hortensis* and apoptotic modulators were analysed. From the results, Piperitol was proved to have strong interaction towards all the apoptotic proteins. Investigation on *in silico* predictions of interactions between bio compounds of *T. flagelliforme* and *K ras* revealed the greater binding efficiency of these compounds to target different allosteric sites of *K ras,* thus blocking the cell signaling pathway in cancer cells (Fatima and Yee, 2014). Computational simulation work done by Muniaraj *et al.* (2018) on the interactions between EGFR and compounds of cyanobacteria predicted the binding affinities of the selected ligands of cyanobacteria towards EGFR.

Thus the findings of the present study revealed that the phytoconstituents of *T. roseo-alba,* selected as ligand molecules based on the preliminary studies, were able to interact efficiently with the apoptotic targets and selected protein molecules involved in lung cancer pathways such as oncogenic proteins, cell signalling molecules and cell surface receptors, thus blocking cell signalling pathway that eventually suppress cancer progression. These *in silico* results would be the platform for the drugs to be focused for *in vitro and in vivo* studies in future for exploring therapeutic strategies against lung cancer.